

DBI inflation with a non-minimally coupled Gauss-Bonnet term

Kourosh Nozari¹ and Narges Rashidi²

Department of Physics, Faculty of Basic Sciences, University of Mazandaran,
P. O. Box 47416-95447, Babolsar, IRAN

Abstract

We study the inflation in a model with a Gauss-Bonnet term which is non-minimally coupled to a DBI field. We study the spectrum of the primordial perturbations in details. The non-Gaussianity of this model is considered and the amplitude of the non-Gaussianity is studied both in the equilateral and orthogonal configurations. By taking various functions of the DBI field, inflaton potential and the Gauss-Bonnet coupling term, we test the model with observational data and find some constraints on the Gauss-Bonnet coupling parameter.

PACS: 04.50.Kd , 98.80.Cq , 98.80.Es

Key Words: Inflation, Cosmological Perturbations, Non-Gaussianity, Non-Minimal Coupling, Observational Constraints.

¹knozari@umz.ac.ir

²n.rashidi@umz.ac.ir

1 Introduction

An inflationary stage in the early time evolution of the universe can address successfully at least some of the problems of the standard big bang cosmology such as the flatness, horizon and relics problems. The simplest inflationary scenario, is the one in which the universe is dominated with a single scalar field whose potential energy dominates over the kinetic term [1, 2, 3, 4, 5, 6, 7, 8]. Another important property of the inflationary paradigm is that, it provides a causal mechanism for production of density perturbations needed to seed the formation of structures in the universe. In a single field inflationary scenario, the dominant mode of the primordial density fluctuations is predicted to be adiabatic and Gaussian to a very good approximation [9]. But, many inflationary models predict a level of non-Gaussianity which is detectable by current experiments [9, 10, 11, 12, 13]. Also, any footprint of the non-Gaussianity in observations carries a large amount of information on the cosmological dynamics which derived the inflationary expansion of the Universe [14, 15]. While the evolution of the primordial fluctuations during inflation is usually studied within the linear theory, to explore the non-Gaussianity of the density perturbation one has to go beyond the linear theory. In fact, one has to study the three-point correlation function of the scalar perturbations or its Fourier transform called the bispectrum. For a Gaussian signal, all odd n -point correlation functions are vanishing. Also, the higher even n -point correlators are given in terms of the sums of the products of the two-point functions. So, in order to look for a departure from Gaussianity we should look for a non-zero three-point correlation functions. To study the three-point correlation functions, it is required a perturbative treatment up to the second order [8, 10, 16, 17]. So, a non-Gaussian distribution of the perturbations implies non-linearity in the cosmological perturbations. A three-point correlation function, in the Fourier space, depends on the three momenta or wave numbers (k_1 , k_2 and k_3). Because of the translation invariance, these momenta add up to zero ($k_1 + k_2 + k_3 = 0$) and thus form a triangle. Also, the rotational invariance implies that the three-point correlation function depends on the three independent scalar products of these momenta (or the shape of the triangle) [14, 18, 19, 20, 21].

It is believed that Einstein gravity is a low-energy limit of a quantum theory of gravity. String theory is the leading candidate for quantum gravity. This theory suggests that to have a ghost-free action, quadratic curvature corrections to the Einstein-Hilbert action is proportional to the Gauss-Bonnet term ($R_{abcd}R^{abcd} - 4R_{ab}R^{ab} + R^2$). Such term plays a significant role in the early time Universe dynamics [22, 23]. However it turns out that this term makes no contribution in the equation for dimension < 5 . But, any coupling between a scalar field and the Gauss-Bonnet term makes the Gauss-Bonnet term effective even in four dimension [24, 25, 26, 27]. For higher dimensional extensions see for instance [28, 29, 30, 31, 32, 33, 34].

There is another proposal in the string theory that has attracted much attention over the past years. In this proposal (which is based on the Dirac-Born-Infeld (DBI) action [35, 36]), the inflaton field is identified with radial coordinate (position) of a D3 brane moving in a “throat” region of a warped compactified space with a speed limit imposed upon its motion, affected by both its speed and the warp factor of the throat (often assumed an AdS_5 throat). The effective action in this model involves a non-standard kinetic term and a function of the scalar field besides the potential which is related to the local geometry of the compact manifold traversed by the D3-brane [35]. An interesting phenomenological feature of the DBI inflation is that it leads to the non-Gaussian signatures in the Cosmic Microwave Background [37, 38].

Based on these preliminaries, in this paper we consider a Gauss-Bonnet term in the action that is non-minimally coupled to the DBI field. After obtaining the main equations of the model, we study

cosmological inflation and the primordial perturbations with details in this setup. Also, the issue of non-Gaussianity of the perturbations will be considered and the amplitude of the non-Gaussianity in the equilateral and orthogonal configuration will be calculated. Finally we perform a comparison between the inflationary parameters and the joint Planck+WMAP9+BAO data [39, 40]. By this comparison we find some constraint on the Gauss-Bonnet coupling parameter α_{GB} .

2 The Setup

The 4-dimensional action for a DBI model in the presence of the Gauss-Bonnet term, which is non-minimally coupled to the DBI field, can be written as follows

$$S = \int \sqrt{-g} \left[\frac{1}{\kappa^2} R - f^{-1}(\phi) \sqrt{1 - f(\phi) \partial_\alpha \phi \partial^\alpha \phi} - V(\phi) + \alpha(\phi) \mathcal{L}_{GB} \right] d^4x, \quad (1)$$

where R is the 4-dimensional Ricci scalar, ϕ is the DBI field and $V(\phi)$ is its potential. $f^{-1}(\phi)$, which is the inverse brane tension, is related to the geometry of the throat. $\alpha(\phi)$ is a potential term which is coupled to the Gauss-Bonnet term. Also, \mathcal{L}_{GB} , the lagrangian term corresponding to the Gauss-Bonnet effect, is given by

$$\mathcal{L}_{GB} = R^2 - 4R_{\mu\nu}R^{\mu\nu} + R_{\mu\nu\alpha\beta}R^{\mu\nu\alpha\beta}. \quad (2)$$

Einstein's field equations obtained from action (1) are given by the following expression

$$G_{\mu\nu} = \kappa^2 T_{\mu\nu} + \kappa^2 \mathcal{T}_{\mu\nu}, \quad (3)$$

where $T_{\mu\nu}$, the energy momentum tensor corresponding to the DBI field is given by

$$T_{\mu\nu} = -\frac{\partial_\mu \phi \partial_\nu \phi}{\sqrt{1 - f(\phi) \partial_\alpha \phi \partial^\alpha \phi}} + g_{\mu\nu} \left(-f^{-1}(\phi) \sqrt{1 - f(\phi) \partial_\alpha \phi \partial^\alpha \phi} + f^{-1}(\phi) - V(\phi) \right), \quad (4)$$

and $\mathcal{T}_{\mu\nu}$ is the energy momentum tensor corresponding to the Gauss-Bonnet term, given by

$$\begin{aligned} \mathcal{T}^{\mu\nu} = & \frac{1}{2} g^{\mu\nu} \alpha(\phi) \mathcal{L}_{GB} - 2\alpha(\phi) R R^{\mu\nu} + 4\alpha(\phi) R_\rho^\mu R^{\nu\rho} - 2\alpha(\phi) R^{\mu\rho\sigma\tau} R_{\rho\sigma\tau}^\nu - 4\alpha(\phi) R^{\mu\rho\sigma\nu} R_{\rho\sigma} \\ & + 2 \left[\nabla^\mu \nabla^\nu \alpha(\phi) \right] R - 2g^{\mu\nu} \left[\nabla^2 \alpha(\phi) \right] R - 4 \left[\nabla_\rho \nabla^\mu \alpha(\phi) \right] R^{\nu\rho} - 4 \left[\nabla_\rho \nabla^\nu \alpha(\phi) \right] R^{\mu\rho} + 4 \left[\nabla^2 \alpha(\phi) \right] R^{\mu\nu} \\ & + 4g^{\mu\nu} \left[\nabla_\rho \nabla_\sigma \alpha(\phi) \right] R^{\rho\sigma} - 4 \left[\nabla_\rho \nabla_\sigma \alpha(\phi) \right] R^{\mu\rho\sigma\nu}. \end{aligned} \quad (5)$$

The total energy momentum tensor ($T_{\mu\nu} + \mathcal{T}_{\mu\nu}$) leads to the following energy density and pressure for this model

$$\rho = \frac{-f^{-1} \sqrt{1 - f\dot{\phi}^2} + f^{-1}}{\sqrt{1 - f\dot{\phi}^2}} + V - 12H^3 \alpha' \dot{\phi}, \quad (6)$$

$$p = -f^{-1} \sqrt{1 - f\dot{\phi}^2} + f^{-1} - V - 12H^2 (\alpha'' \dot{\phi}^2 + \alpha' \ddot{\phi}) - 24H\dot{H} \alpha' \dot{\phi} - 24H^3 \alpha' \dot{\phi}, \quad (7)$$

where, a dot shows derivative with respect to the time and a prime marks derivative with respect to the DBI field. By assuming the following spatially flat FRW line element

$$ds^2 = -n^2(t)dt^2 + a^2(t)\gamma_{ij}dx^i dx^j, \quad (8)$$

where γ_{ij} is a maximally symmetric 3-dimensional metric defined as $\gamma_{ij} = \delta_{ij} + k \frac{x_i x_j}{1 - k r^2}$ where $k = -1, 0, +1$ parameterizes the spatial curvature and $r^2 = x_i x^i$. We assume $n^2(t) = 1$ and consider the $(0, 0)$ component of the Einstein's field equations in order to obtain the Friedmann equation for this model as

$$H^2 = \frac{\kappa^2}{3} \left[\frac{-f^{-1} \sqrt{1 - f \dot{\phi}^2} + f^{-1}}{\sqrt{1 - f \dot{\phi}^2}} + V + 12H^3 \alpha' \dot{\phi} \right]. \quad (9)$$

By varying the action (1) with respect to the scalar field we reach the following equation of motion

$$\frac{\ddot{\phi}}{(1 - f \dot{\phi}^2)^{\frac{3}{2}}} + \frac{3H\dot{\phi}}{(1 - f \dot{\phi}^2)^{\frac{1}{2}}} - V' = -f' f^{-2} \left[1 + \sqrt{1 - f \dot{\phi}^2} - \frac{1}{2} \frac{f \dot{\phi}^2}{\sqrt{1 - f \dot{\phi}^2}} \right] + 12\alpha' H^2 (\dot{H} + H^2). \quad (10)$$

If we consider the slow-roll approximation, where $\dot{\phi}^2 \ll 1$ and $\ddot{\phi} \ll |3H\dot{\phi}|$, the energy density and the equation of motion of the DBI field take the following forms respectively

$$\rho = V - 12H^3 \alpha' \dot{\phi}, \quad (11)$$

and

$$3H\dot{\phi} - V' + 2f' f^{-2} - \alpha' R_{GB} = 0, \quad (12)$$

where

$$R_{GB} = 12H^2 (\dot{H} + H^2). \quad (13)$$

In this regard, the Friedmann equation of the model (9) reduces to the following expression

$$H^2 = \frac{\kappa^2}{3} \left[V - 12H^3 \alpha' \dot{\phi} \right]. \quad (14)$$

The slow-roll parameters which are defined by $\epsilon \equiv -\frac{\dot{H}}{H^2}$ and $\eta \equiv -\frac{1}{H} \frac{\ddot{H}}{\dot{H}}$, in this model take the following forms respectively

$$\epsilon = \frac{1}{2\kappa^2} \frac{V'^2}{V^2} \frac{\frac{2f'f^{-2}}{V'} - 1 - \alpha' R_{GB} V'}{\left(1 - \frac{4\kappa^2}{3} \alpha' (V' - 2f'f^{-2} + \alpha' R_{GB})\right)^2} \left[\frac{1}{1 - \frac{4\kappa^2}{3} \alpha' (V' - 2f'f^{-2} + \alpha' R_{GB})} - \frac{4V}{3V'} X \right], \quad (15)$$

where

$$X = \frac{\alpha'' (V' - 2f'f^{-2} + \alpha' R_{GB}) + \alpha' (V'' - 2f''f^{-2} + 4f'^2 f^{-3} + \alpha'' R_{GB})}{\left(1 - \frac{4\kappa^2}{3} \alpha' (V' - 2f'f^{-2} + \alpha' R_{GB})\right)^2}, \quad (16)$$

and

$$\eta = -\frac{2\dot{Y}}{HY} - \frac{1}{3H^2 \alpha'} \frac{1 - Z}{Z} \left[\alpha'' (V' - 2f'f^{-2} + \alpha' R_{GB}) + \alpha' (V'' - 2f''f^{-2} + 4f'^2 f^{-3} + \alpha'' R_{GB}) \right], \quad (17)$$

where

$$Y = \left[V' - 2f'f^{-2} + \alpha' R_{GB} \right] \times \left[\frac{\kappa^2 V'}{9H} + \frac{4\kappa^2}{9} \alpha'' (V' - 2f'f^{-2} + \alpha' R_{GB}) + \frac{4\kappa^2}{9} \alpha' (V'' - 2f''f^{-2} + 4f'^2 f^{-3} + \alpha'' R_{GB}) \right], \quad (18)$$

and

$$Z = 1 - \frac{4\kappa^2}{3} \alpha' (V' - 2f'f^{-2} + \alpha' R_{GB}) \quad (19)$$

The inflation takes place under the condition for which $\{\epsilon, \eta\} < 1$; as soon as one of these slow-roll parameters reaches the unity, the inflationary phase terminates.

The number of e-folds during inflation is defined as

$$N = \int_{t_{hc}}^{t_f} H dt, \quad (20)$$

which, in our setup and within the slow-roll approximation can be expressed as

$$N \simeq \int_{\phi_{hc}}^{\phi_f} \frac{3H^2}{V' - 2f'f^{-2} + \alpha' R_{GB}} d\phi, \quad (21)$$

where ϕ_{hc} denotes the value of the field when the universe scale observed today crosses the Hubble horizon during inflation and ϕ_f is the value of the field when the universe exits the inflationary phase. In a model with a DBI field which is non-minimally coupled to the Gauss-Bonnet term, the number of e-folds in the slow-roll approximation takes the following form

$$N \simeq - \int_{\phi_{hc}}^{\phi_f} \frac{\kappa^2 V \left[1 - \frac{4\kappa^2}{3} \alpha' (V' - 2f'f^{-2} + \alpha' R_{GB}) \right]^{-1}}{V' - 2f'f^{-2} + \alpha' R_{GB}} d\phi. \quad (22)$$

In the next section, we study the scalar perturbation of the metric (the density perturbation) with details.

3 Perturbations

In this section, we study the linear perturbation theory in the presence of the DBI field and the Gauss-Bonnet term in the action. Among many different ways, depending on the choice of gauge (coordinates) characterizing the cosmological perturbations, we choose the longitudinal gauge in which the scalar metric perturbations of the FRW background are given by [41, 42, 43]

$$ds^2 = -(1 + 2\Phi)dt^2 + a^2(t)(1 - 2\Psi)\delta_{ij} dx^i dx^j, \quad (23)$$

where $a(t)$ is the scale factor, $\Phi = \Phi(t, x)$ and $\Psi = \Psi(t, x)$, the metric perturbations, are gauge-invariant variables. The form of the spatial dependence of all perturbed quantities is similar to the plane waves e^{ikx} , where k is the wave number. Any perturbation of the metric, through Einstein's

field equations, leads to the perturbation in the energy-momentum tensor. For the perturbed metric (23), the perturbed Einstein's field equations can be obtained as follows

$$-6H(H\Phi + \dot{\Psi}) - \frac{2k^2}{a^2} = \kappa^2 \frac{f'\delta\phi}{f^2} \left(1 - \frac{1}{\sqrt{1 - \dot{\phi}^2}}\right) + \kappa^2 \frac{f'\dot{\phi}^2\delta\phi - 2f\dot{\phi}\dot{\delta\phi} - 2f\dot{\phi}^2\Phi}{2f(1 - f\dot{\phi}^2)^{\frac{3}{2}}} + \kappa^2 V'\delta\phi + \kappa^2 \delta\rho_{GB}, \quad (24)$$

$$2\ddot{\Psi} + 6H(H\Phi + \dot{\Psi}) + 2H\dot{\Phi} + 4\dot{H}\Phi + \frac{2}{3a^2}k^2(\Phi - \Psi) = \kappa^2 \frac{f'\delta\phi}{f^2} \left(\sqrt{1 - f\dot{\phi}^2} - 1\right) + \kappa^2 \frac{f'\dot{\phi}^2\delta\phi - 2f\dot{\phi}\dot{\delta\phi} - 2f\dot{\phi}^2\Phi}{2f\sqrt{1 - f\dot{\phi}^2}} - \kappa^2 V'\delta\phi + \kappa^2 \delta p_{GB}, \quad (25)$$

$$\dot{\Psi} + H\Phi = -\frac{\kappa^2 V(\phi)}{\sqrt{1 - \dot{\phi}^2}} \frac{\dot{\phi}\delta\phi}{2} + 4H^2(\alpha''\dot{\phi} + \alpha'\ddot{\phi})\delta\phi - 4H^3\alpha'\delta\phi - \frac{8H}{3}\alpha'\dot{\phi}(3H\Phi - 3\dot{\Psi}) - 4H^2\alpha'\dot{\phi}\Phi, \quad (26)$$

$$\Psi - \Phi = -4(\alpha''\dot{\phi}^2 + \alpha'\ddot{\phi})\Psi - 4H\alpha'\dot{\phi}\Phi - 4(\dot{H} + H^2)\alpha'\delta\phi. \quad (27)$$

As we see from equation (27), in the model with non-minimal coupling between the DBI field and the Gauss-Bonnet term, the two metric perturbations are not equal. In equations (24) and (25), the perturbed energy density and pressure of the Gauss-Bonnet term are given by the following expression

$$\delta\rho_{GB} = -12H^3(\alpha''\dot{\phi} + \alpha'\ddot{\phi})\delta\phi + 12H^2\alpha'\dot{\phi}(4H\Phi - 3\dot{\Psi}) + 4H\frac{k^2}{a^2}(H\alpha'\delta\phi + 2\alpha'\dot{\phi}\Psi), \quad (28)$$

and

$$\begin{aligned} \delta p_{GB} = & -12H^2\ddot{\alpha} - 24H(\dot{H} + H^2)\alpha'\delta\phi - \frac{8k^2}{a^2}(\dot{H} + H^2)\alpha'\delta\phi + 8H\alpha'\dot{\phi}(3\dot{H}\Phi + 3H\dot{\Phi} - 3\ddot{\Psi}) \\ & + 8(H(\alpha''\dot{\phi}^2 + \alpha'\ddot{\phi}) + \dot{H}\alpha'\dot{\phi} + 3H^2\alpha'\dot{\phi}) + 24H(H(\alpha''\dot{\phi}^2 + \alpha'\ddot{\phi}) + 2\dot{H} + \alpha'\dot{\phi} + H^2\alpha'\dot{\phi})\Phi \\ & - \frac{8k^2}{a^2}((\alpha''\dot{\phi}^2 + \alpha'\ddot{\phi})\Psi + H\alpha'\dot{\phi}\Phi) + 12H^2\alpha'\dot{\phi}\dot{\Phi}, \end{aligned} \quad (29)$$

which are obtained by perturbing the (0,0) and (i,j) components of equation (5). By varying the scalar field's equation of motion (10) we achieve

$$\begin{aligned} \ddot{\delta\phi} + 3H\dot{\delta\phi} + 2V'\Phi - \dot{\phi}(\dot{\Phi} + 3\dot{\Psi}) + f''f^{-2}\left(1 - \frac{1}{2}f\dot{\phi}^2\right)\delta\phi - 2f'^2f^{-3}\left(1 - f\dot{\phi}^2\right)\delta\phi - V''\sqrt{1 - f\dot{\phi}^2} \\ + f'f^{-1}(\dot{\phi}\dot{\delta\phi} + \dot{\phi}^2\Phi) - \frac{f'^2f^2\dot{\phi}^2\delta\phi - 2f'f^{-1}(\dot{\phi}\dot{\delta\phi} + \dot{\phi}^2\Phi) - V'f'\dot{\phi}^2\delta\phi - 2V'f(\dot{\phi}\dot{\delta\phi} - \dot{\phi}^2\Phi)}{2\sqrt{1 - f\dot{\phi}^2}} \\ - 6\alpha'H^2(\dot{H} + H^2)\left[f'\dot{\phi}^2\delta\phi - 2f(\dot{\phi}\dot{\delta\phi} - \dot{\phi}^2\Phi)\right] + \sqrt{1 - f\dot{\phi}^2}\left[2H^2\delta R - 8\dot{H}(H(3H\Phi - 3\dot{\Psi}) - \frac{k^2}{a^2}\Psi)\right] \end{aligned}$$

$$= \frac{f' \delta \phi \ddot{\phi}^2 - 2f \ddot{\phi} \delta \dot{\phi} - 2f^2 \dot{\phi}^3 \ddot{\phi}}{(1 - f\dot{\phi}^2)^2}, \quad (30)$$

where the variation of the Ricci scalar is defined as

$$\delta R = 2 \left[2 \frac{k^2}{a^2} \Psi - (3\dot{H}\Phi + 3H\dot{\Phi} - 3\ddot{\Psi}) - 4H(3H\Phi - 3\dot{\Psi}) - \left(3\dot{H} - \frac{k^2}{a^2} \right) \Phi \right]. \quad (31)$$

One can decompose the scalar perturbations into two parts. One part which is the projection parallel to the trajectory is called adiabatic or curvature perturbations (if there is only one scalar field during the inflationary period, we deal with this type of perturbations [44, 45, 46, 47, 48]). Another part which is the projection orthogonal to the trajectory is dubbed the entropy or isocurvature perturbations (if inflation is driven by more than one scalar field [44, 45, 49, 50] or it interacts with other fields such as the scalar Ricci term [46, 47], we deal with this type of perturbations). In this work, since the DBI field is non-minimally coupled to the Gauss-Bonnet term, the perturbations are expected to be non-adiabatic. To explore the first order cosmological perturbation (linear perturbation), we can define a gauge-invariant primordial curvature perturbation ζ , on scales outside the horizon, as follows [51]

$$\zeta = \Psi - \frac{H}{\dot{\rho}} \delta \rho. \quad (32)$$

The above quantity, on uniform density hypersurfaces where $\delta \rho = 0$, reduces to the curvature perturbation, Ψ . By using the equation (32) one can obtain the following equation for time evolution of ζ [52]

$$\dot{\zeta} = H \left(\frac{\delta p_{nad}}{\rho + p} \right). \quad (33)$$

Equation (33) shows that, independent of the form of the gravitational field equations, any change in the curvature perturbation on uniform-density hypersurfaces, on large scales, is due to the non-adiabatic part of the pressure perturbation. ζ is constant if the pressure perturbation is adiabatic on the large scales. In our setup, since the non-adiabatic perturbation is expected, the curvature perturbation would vary with time.

In general, the pressure perturbation (in any gauge) can be decomposed into adiabatic and entropic (non-adiabatic) parts [52]

$$\delta p = c_s^2 \delta \rho + \dot{p} \Gamma, \quad (34)$$

where $c_s^2 = \frac{\dot{p}}{\dot{\rho}}$ is the sound effective velocity. In equation (34), $\delta p_{nad} = \dot{p} \Gamma$, is the non-adiabatic part, where Γ marks the displacement between hypersurfaces of uniform pressure and density.

In the presence of the non-minimal coupling between the DBI field and the Gauss-Bonnet term, δp_{nad} is not zero anymore. So, from equation (34), we can find the δp_{nad} as follows

$$\begin{aligned} \delta p_{nad} = & \kappa^2 V' (f\dot{\phi}^2 - 2) \delta \phi + \frac{2}{\kappa^2} \left[1 - f\dot{\phi}^2 - D \right] \left[-3H(H\Phi + \dot{\Psi}) - \frac{k^2}{a^2} \right] \\ & - \delta \rho_{GB} (1 - f\dot{\phi}^2) - 2\kappa^2 \frac{f' \delta \phi}{f^2} (1 - f\dot{\phi}^2 - \sqrt{1 - f\dot{\phi}^2}) + \delta p_{GB}, \end{aligned} \quad (35)$$

where

$$D = \frac{f' f^{-2} \dot{\phi} \sqrt{1 - f\dot{\phi}^2} + \frac{2\dot{\phi}\ddot{\phi} + f' f^{-1} \dot{\phi}^3}{\sqrt{1 - f\dot{\phi}^2}} - f' f^{-2} \dot{\phi} - V' \dot{\phi} - \dot{p}_{GB}}{\frac{f' \dot{\phi}}{f^2} - \frac{f' \dot{\phi}}{f^2 \sqrt{1 - f\dot{\phi}^2}} + \frac{f' \dot{\phi}^3 - 2f\dot{\phi}\ddot{\phi}}{2f(1 - f\dot{\phi}^2)^{\frac{3}{2}}} + V' \dot{\phi} + \dot{p}_{GB}}. \quad (36)$$

From equation (33), we find that, this non-vanishing, non-adiabatic pressure leads to the non-vanishing time evolution of the primordial curvature perturbation as follows

$$\dot{\zeta} = \frac{Hf\dot{\phi}^2}{f\dot{\phi}^2 + (\rho_{GB} + p_{GB})f\sqrt{1-f\dot{\phi}^2}} \left\{ \frac{2}{\kappa^2} \left[1 - f\dot{\phi}^2 - D \right] \left[-3H(H\Phi + \dot{\Psi}) - \frac{k^2}{a^2} \right] + \kappa^2 V' (f\dot{\phi}^2 - 2) \delta\phi - \delta\rho_{GB} (1 - f\dot{\phi}^2) - 2\kappa^2 \frac{f'\delta\phi}{f^2} (1 - f\dot{\phi}^2 - \sqrt{1-f\dot{\phi}^2}) + \delta p_{GB} \right\}. \quad (37)$$

We see that, in the presence of the non-minimally coupled Gauss-Bonnet term, the primordial curvature perturbations attain an explicit time-dependence.

The scales of cosmological interest have spent most of their time far outside the Hubble radius and have re-entered only relatively recently in the Universe history. So, in order to obtain scalar and tensorial perturbations in our model, it is enough to consider the slow-roll approximation at the large scales, $k \ll aH$. In this scale, $\dot{\Phi}$, $\ddot{\Psi}$, $\dot{\Phi}$ and $\ddot{\Psi}$ are negligible (see [53, 54, 55, 56]). So, at large scales, the perturbed equation of motion takes the following form

$$3H\delta\dot{\phi} + \left[f''f^{-2} - 2f'^2f^{-3}\delta\phi - V'' \right] \delta\phi + 12\alpha''R_{GB}\delta\phi = -2V'\Phi + 2H^2\delta R - 24\dot{H}H^2\Phi. \quad (38)$$

Also, the perturbed Einstein's field equation (26) gives

$$\Phi = \frac{(4H^2\alpha'' - \kappa^2)\dot{\phi}\delta\phi - 4H^3\alpha'\delta\phi}{2H + 12H^2\alpha'\dot{\phi}}. \quad (39)$$

So, we can rewrite the equation (38) as follows

$$3H\delta\dot{\phi} = \left[V'' - f''f^{-2} + 2f'^2f^{-3} \right] \delta\phi + \left[12H^2(4H^2 - \dot{H}) + 24H\dot{H} - 2V' \right] \frac{(4H^2\alpha'' - \kappa^2)\dot{\phi}\delta\phi - 4H^3\alpha'\delta\phi}{2H + 12H^2\alpha'\dot{\phi}}. \quad (40)$$

In order to solve the equation (40), to obtain the explicit form for the perturbed field $\delta\phi$, we introduce the function \mathcal{A} as

$$\mathcal{A} \equiv \frac{V\delta\phi}{V'}, \quad (41)$$

by which we rewrite equation (40) as follows

$$\frac{\mathcal{A}'}{\mathcal{A}} = \frac{V'}{V} - \frac{V''}{V} + \frac{12\alpha''R_{GB} + V'' - f''f^{-2} + 2f'^2f^{-3}}{\frac{1}{2}\alpha'R_{GB} - 2f'f^{-2} + V'} + \mathcal{D} \quad (42)$$

where

$$\mathcal{D} = \left[12H^2(4H^2 + \epsilon H^2) - 24\epsilon H^3 - 2V' \right] \left[\frac{4H^2\alpha'' - \kappa^2}{6H^2 + 12H^2\alpha'(\frac{1}{2}\alpha'R_{GB} - 2f'f^{-2} + V')} - \frac{4H^3\alpha'}{2H(\frac{1}{2}\alpha'R_{GB} - 2f'f^{-2} + V') + 4H\alpha'(\frac{1}{2}\alpha'R_{GB} - 2f'f^{-2} + V')} \right]. \quad (43)$$

A solution of this equation is given by the following expression

$$\mathcal{A} = \mathcal{C} \exp \left(\int \frac{\mathcal{A}'}{\mathcal{A}} d\varphi \right), \quad (44)$$

where \mathcal{C} is an integration constant. So, from equation (41) we achieve

$$\delta\phi = \frac{\mathcal{C}V'}{V} \exp \left[\int \left(\frac{V'}{V} - \frac{V''}{V} + \frac{12\alpha''R_{GB} + V'' - f''f^{-2} + 2f'^2f^{-3}}{\frac{1}{2}\alpha'R_{GB} - 2f'f^{-2} + V'} + \mathcal{D} \right) d\phi \right]. \quad (45)$$

By using equation (53), we can find the following expression for the density perturbation amplitude

$$A_s^2 = \frac{k^3 \mathcal{C}}{2\pi^2} \frac{V'^2}{V^2} \exp \left[2 \int \left(\frac{V'}{V} - \frac{V''}{V} + \frac{12\alpha''R_{GB} + V'' - f''f^{-2} + 2f'^2f^{-3}}{\frac{1}{2}\alpha'R_{GB} - 2f'f^{-2} + V'} + \mathcal{D} \right) d\phi \right]. \quad (46)$$

The scale-dependence of the perturbations is described by the spectral index as

$$n_s - 1 = \frac{d \ln A_s^2}{d \ln k}. \quad (47)$$

where the interval in wave number is related to the number of e-folds by the relation $d \ln k(\phi) = dN(\phi)$. By using equations (44) and (47), the scalar spectral index becomes

$$\begin{aligned} n_s - 1 = & \frac{1}{3H^2} \left[f''f^{-2} - 12\alpha''R_{GB} - V'' - 2f'^2f^{-3} \right] + \left[24\epsilon H^3 + 2V' - 12H^2(4H^2 + \epsilon H^2) \right] \\ & \times \frac{(4H^2\alpha'' - \kappa^2) \left(\frac{1}{2}\alpha'R_{GB} - 2f'f^{-2} + V' \right) - 12H^4\alpha'}{9H^2(2H + H\alpha'(\frac{1}{2}\alpha'R_{GB} - 2f'f^{-2} + V'))} \end{aligned} \quad (48)$$

Also, the tensor perturbations amplitude of a given mode when leaving the Hubble radius is defined as

$$A_T^2 = \frac{4\kappa^2}{25\pi} H^2 \Big|_{k=aH}. \quad (49)$$

In a model with a DBI field which is non-minimally coupled to the Gauss-Bonnet term, the tensor perturbations amplitude of a given mode when leaving the Hubble radius is given by

$$A_T^2 = \frac{4\kappa^4 V}{75\pi(1 - \kappa^2 f)} \left[1 - \frac{4\kappa^2}{3} \alpha' (V' - 2f'f^{-2} + \alpha'R_{GB}) \right]^{-1}. \quad (50)$$

So, the tensor spectral index which is defined as

$$n_T = \frac{d \ln A_T^2}{d \ln k}, \quad (51)$$

in this setup takes the following form

$$n_T = \frac{\kappa^2 \dot{\phi}}{3H^2} \left\{ V' \left[\frac{4\kappa^2}{3} \alpha' (V' - 2f'f^{-2} + \alpha'R_{GB}) \right] + V \left[1 - \frac{4\kappa^2}{3} \alpha' (V' - 2f'f^{-2} + \alpha'R_{GB}) \right]^{-2} \right\}$$

$$\times \left[\frac{4\kappa^2}{3} \alpha'' (V' - 2f' f^{-2} + \alpha' R_{GB}) + \frac{4\kappa^2}{3} \alpha' (V'' - 2f'' f^{-2} + 4f'^2 f^{-3} + \alpha'' R_{GB}) \right] \Bigg\}. \quad (52)$$

The ratio between the amplitudes of tensor and scalar perturbations (tensor-to-scalar ratio) is another important parameter which is given by

$$r = \frac{A_T^2}{A_s^2} = \frac{8\kappa^4 \pi}{75k^3 \mathcal{C}} \frac{V^3}{V'^2} \times \frac{\exp \left[-2 \int \left(\frac{V'}{V} - \frac{V''}{V} + \frac{12\alpha'' R_{GB} + V'' - f'' f^{-2} + 2f'^2 f^{-3}}{\frac{1}{2}\alpha' R_{GB} - 2f' f^{-2} + V'} + \mathcal{D} \right) d\phi \right]}{1 - \frac{4\kappa^2}{3} \alpha' (V' - 2f' f^{-2} + \alpha' R_{GB})}. \quad (53)$$

4 Non-Gaussianity

In this section we are going to study the non-Gaussianity of the primordial density perturbation in this model. As we have said in the Introduction, for a Gaussian distribution, the three-point function and also other odd correlation functions are zero. But this is not the case for non-Gaussian distribution. So, to study the primordial non-Gaussianity, we study the three-point correlators. To this end, we should expand the action (1) up to the cubic order in the small fluctuations (which have their origin in the quantum behavior of both the field ϕ and the space-time metric, $g_{\mu\nu}$) around the homogeneous background solution. These cubic terms in lagrangian, lead to a change both in the ground state of the quantum field and non-linearities in the evolution [9]. To compute the Einstein action to the third order, we work in the ADM metric formalism [57]

$$ds^2 = -N^2 dt^2 + h_{ij} (dx^i + N^i dt) (dx^j + N^j dt) \quad (54)$$

where N and N^i are the lapse and shift functions, respectively. It should be noticed that we consider only scalar metric perturbations about the flat FRW background. A general parametrization of the scalar fluctuations in the metric is provided by expanding the lapse function N and the shift vector N^i , as $N = 1 + 2\Phi$ and $N^i = \delta^{ij} \partial_j B$. Note that there is no need to know N or N^i up to the second order. The reason is that the second order equation is multiplied by a factor which vanishes by the first order solution. Also, the contribution of the third order term vanishes because it is multiplied by the constraint equation at the zeroth order (the zeroth order solution obeys the equations of motion) [9, 12, 58]. In which follows, we work in the uniform-field gauge for which $\delta\phi = 0$. This gauge fixes the time-component of a gauge-transformation vector ξ^μ and so h_{ij} can be written as $a^2(t) e^{2\Psi} \delta^{ij}$ [9, 59]. Now, we write the perturbed metric at the linear level, as [41, 42, 43]

$$ds^2 = -(1 + 2\Phi) dt^2 + 2a^2(t) B_{,i} dx^i dt + a^2(t) (1 - 2\Psi) \delta_{ij} dx^i dx^j \quad (55)$$

By expanding the action (1) up to the second order, we obtain

$$\begin{aligned} S_2 = \int dt d^3x a^3 \Bigg[& \left(24H\alpha'\dot{\phi} - \frac{3}{\kappa^2} \right) \dot{\Psi}^2 - \frac{\left(2H\alpha'\dot{\phi} - \frac{2}{\kappa^2} \right)}{a^2} \dot{\Psi} \partial^2 B - \frac{\left(\frac{2H}{\kappa^2} - 24H^2\alpha'\dot{\phi} \right)}{a^2} \Phi \partial^2 B \\ & - \frac{2}{a^2} \left(\frac{1}{\kappa^2} - 8H\alpha'\dot{\phi} \right) \Phi \partial^2 \Psi + \left(\frac{6H}{\kappa^2} - 72H^2\alpha'\dot{\phi} \right) \Phi \dot{\Psi} + \frac{1}{a^2} \left(\frac{1}{\kappa^2} - 8(\alpha''\dot{\phi}^2 + \alpha'\ddot{\phi}) \right) \partial_i \Psi \partial^i \Psi \Bigg] \times \end{aligned}$$

$$\left(48H^3\alpha'\dot{\phi} - \frac{3H^2}{\kappa^2} + \frac{\dot{\phi}^2}{2\sqrt{1-f\dot{\phi}^2}} + \frac{f\dot{\phi}^4}{2(1-f\dot{\phi}^2)^{\frac{3}{2}}}\right)\Phi^2\Big]. \quad (56)$$

By using the above second order equation, we can find the equation of motion of Φ and B respectively as follows

$$\Phi = \frac{2\kappa^{-2} - 16H\dot{\alpha}}{2\kappa^{-2}H - 24H^2\alpha'\dot{\phi}} \dot{\Psi}, \quad (57)$$

$$\frac{1}{a^2}\partial^2 B = \frac{2\left(48H^3\alpha'\dot{\phi} - \frac{3H^2}{\kappa^2} + \frac{\dot{\phi}^2}{2\sqrt{1-f\dot{\phi}^2}} + \frac{f\dot{\phi}^4}{2(1-f\dot{\phi}^2)^{\frac{3}{2}}}\right)}{3\left(\frac{2H}{\kappa^2} - 24H^2\alpha'\dot{\phi}\right)}\Phi + 3\dot{\Psi} - \frac{2\left(24H\alpha'\dot{\phi} - \frac{3}{\kappa^2}\right)}{a^2\left(\frac{2H}{\kappa^2} - 24H^2\alpha'\dot{\phi}\right)}\partial^2\Psi. \quad (58)$$

By substituting the constraint (57) into the action (56), we find

$$S_2 = \int dt d^3x a^3 \mathcal{U} \left[\dot{\Psi} - \frac{c_s^2}{a^2} (\partial\Psi)^2 \right], \quad (59)$$

where

$$\mathcal{U} = \frac{\left(\frac{1}{\kappa^2} - 8H\dot{\alpha}\right)\left(\left(\frac{4}{\kappa^2} - 32H\dot{\alpha}\right)\left(144H^3\dot{\alpha} - \frac{9H^2}{\kappa^2} + \frac{3\dot{\phi}^2}{2\sqrt{1-f\dot{\phi}^2}} + \frac{3f\dot{\phi}^4}{2(1-f\dot{\phi}^2)^{\frac{3}{2}}}\right) + 9\left(\frac{2H}{\kappa^2} - 24H^2\dot{\alpha}\right)\right)}{3\left(\frac{2H}{\kappa^2} - 24H\dot{\alpha}\right)^2}, \quad (60)$$

and

$$c_s^2 = \frac{3\left(\left(\frac{2}{\kappa^2} - 16H\dot{\alpha}\right)\left(\frac{2H}{\kappa^2} - 24H^2\dot{\alpha}\right)H - \left(\frac{8H}{\kappa^2} - 96H^2\dot{\alpha}\right)\left(8\dot{H}\dot{\alpha} + 8H\ddot{\alpha}\right)\right)}{\left(\frac{4}{\kappa^2} - 32H\dot{\alpha}\right)\left(144H^3\dot{\alpha} - \frac{9H^2}{\kappa^2} + \frac{3\dot{\phi}^2}{2\sqrt{1-f\dot{\phi}^2}} + \frac{3f\dot{\phi}^4}{2(1-f\dot{\phi}^2)^{\frac{3}{2}}}\right) + 9\left(\frac{2H}{\kappa^2} - 24H\dot{\alpha}\right)^2} \\ - \frac{\frac{3\left(\frac{2H}{\kappa^2} - 24H^2\dot{\alpha}\right)^2}{\frac{1}{\kappa^2} - 8H\dot{\alpha}}\left(\frac{1}{\kappa^2} - 8\ddot{\alpha}\right) + \left(\frac{2}{\kappa^2} - 16H\dot{\alpha}\right)\left(\frac{2\dot{H}}{\kappa^2} - 48H\dot{H}\dot{\alpha} - 24H^2\ddot{\alpha}\right)}{\left(\frac{4}{\kappa^2} - 32H\dot{\alpha}\right)\left(144H^3\dot{\alpha} - \frac{9H^2}{\kappa^2} + \frac{3\dot{\phi}^2}{2\sqrt{1-f\dot{\phi}^2}} + \frac{3f\dot{\phi}^4}{2(1-f\dot{\phi}^2)^{\frac{3}{2}}}\right) + 9\left(\frac{2H}{\kappa^2} - 24H\dot{\alpha}\right)^2}. \quad (61)$$

For more details to obtain the equations of this section, one can refer to [12, 13, 15, 60]. Since our aim in this section is the study of the three-point correlation function of the perturbations, we should expand the action (59) up to the third order. The explicit form of the third-order action is given in the Appendix A. To proceed, we introduce the parameter \hat{B} which, by using equation (58), relates two perturbation parameters as follows

$$B = -\frac{2\kappa^{-2} - 16H\dot{\alpha}}{2\kappa^{-2}H - 24H^2\alpha'\dot{\phi}} + \hat{B}, \quad \partial^2 \hat{B} = \frac{a^2 \mathcal{U} \dot{\Psi}}{\kappa^{-2} - 8H\dot{\alpha}}. \quad (62)$$

On the other hand, the variation of the Lagrangian of action (56) with respect to Ψ , gives us the equation of motion of Ψ as follows

$$\frac{d}{dt}\left(a^3 \mathcal{U} \dot{\Psi}\right) - a \mathcal{U} c_s^2 \partial^2 \Psi = 0. \quad (63)$$

Now, by using equations (57)-(63), we can rewrite the cubic action up to the leading order as follows

$$S_3 = \int dt d^3x \left\{ 3a^3 \left[\mathcal{U} \left(1 - \frac{1}{c_s^2} \right) \right] \Psi \dot{\Psi}^2 + a \left[c_s^2 \mathcal{U} \left(\frac{1}{c_s^2} - 1 \right) \right] \Psi (\partial \Psi)^2 + a^3 \left[\frac{\mathcal{U}}{\kappa H} \left(\frac{1}{c_s^2} - 1 - \frac{2\lambda}{\chi} \right) \right] \dot{\Psi}^3 \right\}. \quad (64)$$

where the parameters λ and χ are defined respectively as

$$\lambda = \frac{f \dot{\phi}^4}{4(1 - f \dot{\phi}^2)^{\frac{3}{2}}} + \frac{f^2 \dot{\phi}^6}{3(1 - f \dot{\phi}^2)^{\frac{5}{2}}}, \quad (65)$$

$$\chi = \frac{\kappa^4}{4} \mathcal{U} \left(2\kappa^{-2} H - 24 H^2 \dot{\alpha} \right)^2. \quad (66)$$

To calculate the three point correlation function we use the interaction picture where H_{int} is equal to \mathcal{L}_3 (the lagrangian of the cubic action). The vacuum expectation value of Ψ for the three-point operator in the conformal time interval between τ_i and τ_f (i and f denote the beginning and end of the inflation respectively) is given by the following expression

$$\langle \Psi(\mathbf{k}_1) \Psi(\mathbf{k}_2) \Psi(\mathbf{k}_3) \rangle = -i \int_{\tau_i}^{\tau_f} d\tau a \langle 0 | [\Psi(\mathbf{k}_1) \Psi(\mathbf{k}_2) \Psi(\mathbf{k}_3), H_{int}] | 0 \rangle. \quad (67)$$

By solving the integral of equation (67), we find the three-point correlation function as follows [15, 60, 61]

$$\langle \Psi(\mathbf{k}_1) \Psi(\mathbf{k}_2) \Psi(\mathbf{k}_3) \rangle = (2\pi)^3 \delta^3(\mathbf{k}_1 + \mathbf{k}_2 + \mathbf{k}_3) \mathcal{B}_\Psi. \quad (68)$$

where

$$\mathcal{B}_\Psi = \frac{H^4 \mathcal{G}_\Psi(k_1, k_2, k_3)}{4 \mathcal{U}^2 c_s^6 \prod_{i=1}^3 k_i^3}. \quad (69)$$

Note that, in solving the integral of equation (67), the coefficients in the bracket are considered as constant [12, 15]. This is because, these coefficients would varies slower than the scale factor. In equation (69), the parameter \mathcal{G}_Ψ is given by the following expression

$$\mathcal{G}_\Psi = \frac{3}{4} \left(1 - \frac{1}{c_s^2} \right) \mathcal{S}_1 + \frac{1}{4} \left(1 - \frac{1}{c_s^2} \right) \mathcal{S}_2 + \frac{3\kappa}{2} \left(\frac{1}{c_s^2} - 1 - \frac{2\lambda}{\chi} \right) \mathcal{S}_3. \quad (70)$$

where K is defined as $K = \sum_i k_i$ and the shape functions \mathcal{S}_1 , \mathcal{S}_2 and \mathcal{S}_3 are defined respectively as

$$\mathcal{S}_1 = \frac{2}{K} \sum_{i>j} k_i^2 k_j^2 - \frac{1}{K^2} \sum_{i \neq j} k_i^2 k_j^3 \quad (71)$$

$$\mathcal{S}_2 = \frac{1}{2} \sum_i k_i^3 + \frac{2}{K} \sum_{i>j} k_i^2 k_j^2 - \frac{1}{K^2} \sum_{i \neq j} k_i^2 k_j^3 \quad (72)$$

and

$$\mathcal{S}_3 = \frac{(k_1 k_2 k_3)^2}{K^3}. \quad (73)$$

There are different shapes, depending on the values of momenta. The momenta form a triangle and each shape has a pick in a configuration of triangle. A local shape [62, 63, 52, 65] has a peak in the squeezed limit (i.e., the limit where the modulus of the momenta approaches $k_3 \ll k_1 \simeq k_2$).

Another shape which is corresponding to the equilateral configuration [66], has a peak at $k_1 = k_2 = k_3$. There is another shape which is orthogonal [67] to equilateral one. A linear combination of the equilateral and orthogonal templates gives a shape which is corresponding to folded triangle [38] and has a pick in $k_1 = 2k_2 = 2k_3$. An orthogonal non-Gaussianity has a signal with a positive peak at the equilateral configuration and a negative peak at the folded configuration. There is a parameter f_{NL} which is called “nonlinearity parameter” [52, 62, 65, 66] and measures the amplitude of the non-Gaussianity. This dimensionless parameter is defined by the following relation

$$f_{NL} = \frac{10}{3} \frac{\mathcal{G}_\Psi}{\sum_{i=1}^3 k_i^3}. \quad (74)$$

Now, we study the amplitude of the non-Gaussianity in the equilateral and orthogonal configurations. To this end, we follow [68] and introduce a shape \mathcal{S}_*^{equil} as

$$\mathcal{S}_*^{equil} = -\frac{12}{13} (3\mathcal{S}_1 - \mathcal{S}_2). \quad (75)$$

There is another shape which is exactly orthogonal to (75) and is defined as [68]

$$\mathcal{S}_*^{ortho} = \frac{12}{14 - 13\beta} (\beta(3\mathcal{S}_1 - \mathcal{S}_2) + 3\mathcal{S}_1 - \mathcal{S}_2), \quad (76)$$

where $\beta \simeq 1.1967996$. So, we can express the leading-order bispectrum (70), in terms of the equilateral basis \mathcal{S}_*^{equil} and the orthogonal basis \mathcal{S}_*^{ortho} , as

$$\mathcal{G}_\Psi = \mathcal{C}_1 \mathcal{S}_*^{equil} + \mathcal{C}_2 \mathcal{S}_*^{ortho}, \quad (77)$$

where

$$\mathcal{C}_1 = \frac{13}{12} \left[\frac{1}{24} \left(1 - \frac{1}{c_s^2} \right) (2 + 3\beta) + \frac{\lambda}{12\chi} (2 - 3\beta) \right], \quad (78)$$

and

$$\mathcal{C}_2 = \frac{14 - 13\beta}{12} \left[\frac{1}{8} \left(1 - \frac{1}{c_s^2} \right) - \frac{\lambda}{4\chi} \right]. \quad (79)$$

In equations (78) and (79), λ and χ are defined by (65) and (66) respectively. By using equations (74) and (77), we obtain

$$f_{NL}^{equil} = \frac{130}{36 \sum_{i=1}^3 k_i^3} \left[\frac{1}{24} \left(1 - \frac{1}{c_s^2} \right) (2 + 3\beta) + \frac{\lambda}{12\chi} (2 - 3\beta) \right] \mathcal{S}_*^{equil}, \quad (80)$$

and

$$f_{NL}^{ortho} = \frac{140 - 130\beta}{36 \sum_{i=1}^3 k_i^3} \left[\frac{1}{8} \left(1 - \frac{1}{c_s^2} \right) - \frac{\lambda}{4\chi} \right] \mathcal{S}_*^{ortho}. \quad (81)$$

As we have stated previously, the shape function in the equilateral configuration has a pick at $k_1 = k_2 = k_3$. Also an orthogonal non-Gaussianity has a signal with a positive peak at the equilateral configuration. So, equations (80) and (81) in the case with $k_1 = k_2 = k_3$ give

$$f_{NL}^{equil} = \frac{325}{18} \left[\frac{1}{24} \left(\frac{1}{c_s^2} - 1 \right) (2 + 3\beta) + \frac{\lambda}{12\chi} (2 - 3\beta) \right], \quad (82)$$

and

$$f_{NL}^{ortho} = \frac{10}{9} \left(\frac{65}{4} \beta + \frac{7}{6} \right) \left[\frac{1}{8} \left(1 - \frac{1}{c_s^2} \right) - \frac{\lambda}{4\chi} \right]. \quad (83)$$

After obtaining the main equations of this setup, in the next section we test this model in confrontation with recent observational data to obtain some constraints on the model's parameters. Our focus is mainly on the coefficient of the Gauss-Bonnet term.

5 Observational Constraints

In the cosmological equations of this model, there are three functions of the DBI field which have important role in the dynamics of the model. These are $f(\phi)$, $V(\phi)$ and $\alpha(\phi)$. Usually $f(\phi)$ is given in terms of the warp factor of the AdS-like throat. In the pure AdS₅, $f(\phi)$ takes a simple form as $f(\phi) = \beta \phi^{-4}$ [36]. On the other hand, in reference [69], the authors have introduced another function for $f(\phi)$ as $f(\phi) = \beta e^{\kappa\phi}$. So, we first divide this section into two subsections; one with $f(\phi) = \beta \phi^4$ and the other with $f(\phi) = \beta e^{\kappa\phi}$. Then, we proceed our study by choosing the form of the potential and the Gauss-Bonnet coupling term. Note that we take the Gauss-Bonnet coupling as $\alpha(\phi) = \alpha_{GB} \mathcal{V}(\phi)$. In constraining our model with observational data, we focus mainly on α_{GB} .

5.1 $f(\phi) = \beta \phi^{-4}$

For this type of $f(\phi)$, we consider three types of potentials: quadratic potential ($V = \frac{\sigma}{2} \phi^2$), quartic potential ($V = \frac{\sigma}{4} \phi^4$) and exponential potential ($V(\phi) = \sigma \exp(-\kappa\phi)$). In which follows, we obtain some constraints on the model parameters by analysis of these parameters in the background of the Planck+WMAP9+ BAO data.

5.1.1 $V(\phi) = \frac{\sigma}{2} \phi^2$

In the first step, we consider a quadratic potential and adopt three functions for $\mathcal{V}(\phi)$ as $\mathcal{V}(\phi) \sim \phi^2$, ϕ^4 and $e^{-\kappa\phi}$. With these choices, we solve the integral of equation (22). For $\mathcal{V}(\phi) \sim \phi^2$, solving the integral gives

$$N = -\frac{1}{64} \kappa^2 \sigma \beta \ln \left(-3\beta + 8\kappa^2 \alpha_{GB} \phi^2 \sigma \beta + 64\kappa^2 \alpha_{GB} \phi^4 + 16\kappa^2 \alpha_{GB}^2 \phi^2 R_{GB} \beta \right) - \frac{1}{32} \kappa^4 \sigma^2 \beta^2 \alpha_{GB} \dot{A} \\ - \frac{1}{16} \kappa^4 \sigma \beta^2 \alpha_{GB}^2 R_{GB} \dot{A} + \frac{1}{32} \kappa^2 \sigma \beta \ln \left(\sigma \beta + 8 \phi^2 + 2 \alpha_{GB} R_{GB} \beta \right) \Big|_{hc}^f, \quad (84)$$

where

$$\dot{A} = \frac{\arctan \left(\frac{1}{8} \frac{8\kappa^2 \alpha_{GB} \sigma \beta + 128\kappa^2 \alpha_{GB} \phi^2 + 16\kappa^2 \alpha_{GB}^2 R_{GB} \beta}{\sqrt{12\kappa^2 \alpha_{GB} \beta + \kappa^4 \alpha_{GB}^2 \sigma^2 \beta^2 + 4\kappa^4 \alpha_{GB}^3 \sigma \beta^2 R_{GB} + 4\kappa^4 \alpha_{GB}^4 R_{GB}^2 \beta^2}} \right) R_{GB}}{\sqrt{12\kappa^2 \alpha_{GB} \beta + \kappa^4 \alpha_{GB}^2 \sigma^2 \beta^2 + 4\kappa^4 \alpha_{GB}^3 \sigma \beta^2 R_{GB} + 4\kappa^4 \alpha_{GB}^4 R_{GB}^2 \beta^2}}. \quad (85)$$

If we set Eq. (15) equal to 1 (corresponding to the end of inflation), we obtain ϕ_f . Then, by substituting this result into equation (84) we find ϕ_{hc} . By substituting ϕ_{hc} into the equations (48) and (53), we plot the tensor to scalar ratio versus the spectral index (the left panel of figure 1). The figure has been plotted for $N = 50$ (the thinner line) and $N = 60$ (the thicker line) (this convention is applied through this paper) in the background of the Planck+WMAP9+BAO joint

data. In all of the figures, the dashed lines are corresponding to $\mathcal{V}(\phi) \sim \phi^2$. As we see from this figure, for some values of α_{GB} , the model is compatible with observational data. In this case, for $N = 50$, the model is compatible with the joint 95% CL of the Planck+WMAP9+BAO data if $3 \times 10^{-4} \leq \alpha_{GB} < 4.2 \times 10^{-3}$. Also, for $N = 60$ this model is compatible with observational data if $2.9 \times 10^{-4} < \alpha_{GB} < 3.65 \times 10^{-3}$. The right panel of figure 1 shows the amplitude of the non-Gaussianity in the orthogonal configuration versus the amplitude of the non-Gaussianity in the equilateral configuration in the background of 68%, 95% and 99% CL of the Planck+WMAP9+BAO data. To plot this figure, we substitute ϕ_{hc} in equations (82) and (83). Here also, the figure has been plotted for $N = 50$ (the thinner line) and $N = 60$ (the thicker line). For $\mathcal{V}(\phi) \sim \phi^2$ and for $N = 50$, the model is compatible with the joint 95% CL of the Planck+WMAP9+BAO data if $3.1 \times 10^{-4} < \alpha_{GB} < 3.74 \times 10^{-3}$. Also, for $N = 60$ it is compatible with observation, if $3 \times 10^{-4} \leq \alpha_{GB} \leq 3.96 \times 10^{-3}$. With this type of \mathcal{V} , the model is well inside the 99% CL of the Planck+WMAP9+BAO data if $2.8 \times 10^{-4} < \alpha_{GB} < 4.14 \times 10^{-3}$ for $N = 50$ and $2.71 \times 10^{-4} \leq \alpha_{GB} \leq 4.22 \times 10^{-3}$ for $N = 60$.

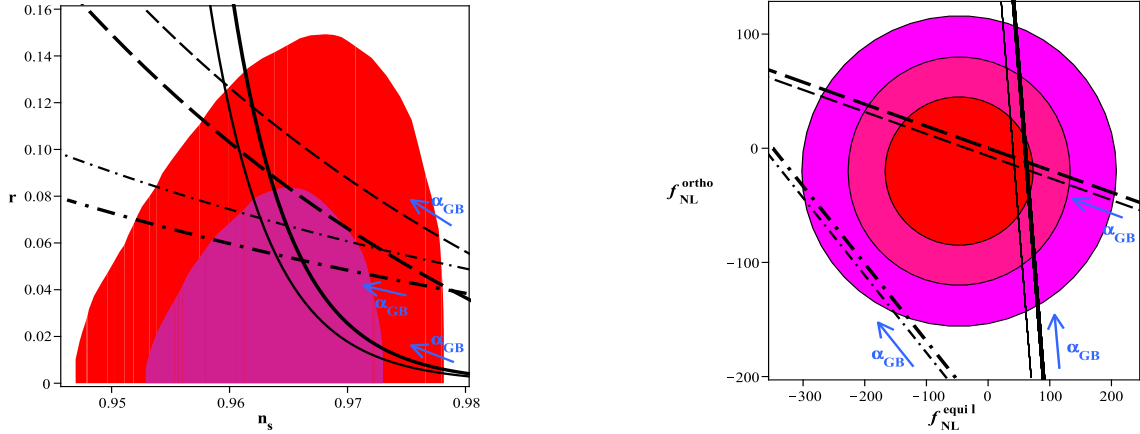


Figure 1: Evolution of the tensor to scalar ratio versus the spectral index (left panel) and the amplitude of the non-Gaussianity in the orthogonal configuration versus the equilateral configuration (right panel), for the case with $f(\phi) = \beta\phi^{-4}$ and with a quadratic potential, in the background of the Planck+WMAP9+BAO data. The figure has been plotted for $N = 50$ (the thinner line) and 60 (the thicker line). The solid lines are corresponding to $\mathcal{V}(\phi) \sim e^{-\kappa\phi}$, the dashed lines are corresponding to $\mathcal{V}(\phi) \sim \phi^2$ and the dash-dotted lines are corresponding to $\mathcal{V}(\phi) \sim \phi^4$. For the both values of N , a model with a non-minimal coupling between the Gauss-Bonnet term and the DBI field, in some ranges of α_{GB} is compatible with observational data.

Now, we adopt $\mathcal{V}(\phi) \sim \phi^4$ and solve the integral of equation (22). The result is given by the following expression

$$N = \frac{4}{9} \kappa^4 \sigma \alpha_{GB} \phi^6 + \frac{1}{4} \frac{\kappa^2 \sigma \beta \ln(\sigma \beta + 8\phi^2 + 4\alpha_{GB} \phi^2 R_{GB} \beta)}{8 + 4\alpha_{GB} R_{GB} \beta} \Big|_{hc}^f, \quad (86)$$

By finding ϕ_{hc} from this equation, we can plot the evolution of the tensor to scalar ratio versus the spectral index (the dash-dotted lines in the left panel of figure 1) by using of equations (48) and (53). For $\mathcal{V}(\phi) \sim \phi^4$ and for $N = 50$, this model is inside the joint 95% CL of the Planck+WMAP9+BAO

data if $6 \times 10^{-4} < \alpha_{GB} < 2.44 \times 10^{-3}$. For $N = 60$ this model is compatible with observation if $6.23 \times 10^{-4} < \alpha_{GB} < 2.524 \times 10^{-3}$. In studying the amplitude of the non-Gaussianity we find that for this case, the model both with $N = 50$ and $N = 60$ is outside the 95% CL of the Planck+WMAP9+BAO data. But, for $N = 50$, the model with $5.2 \times 10^{-4} < \alpha_{GB} \leq 3 \times 10^{-3}$ and for $N = 60$, the model with $5.5 \times 10^{-4} < \alpha_{GB} < 3.02 \times 10^{-3}$ lies inside the 99% CL of the Planck+WMAP9+BAO data.

$\mathcal{V} \sim e^{-\kappa\phi}$ is another case that we consider here. By this function, solving the integral of equation (22) gives

$$N = \frac{1}{32} \sigma \kappa^2 \beta \ln \left(\frac{1}{8} \sigma \beta + \phi^2 \right) + \frac{1}{2} \frac{\sigma \kappa^2 \left(\frac{8}{3} \alpha_{GB} + \frac{8}{3} \kappa \alpha_{GB} \phi + \frac{4}{3} \kappa^2 \alpha_{GB} \phi^2 \right)}{e^{\kappa\phi}} + \frac{1}{2} \frac{\sigma \left(\kappa^2 \phi^2 e^{\kappa\phi} - 2\kappa\phi e^{\kappa\phi} + 2e^{\kappa\phi} \right)}{\kappa^2 R_{GB} \alpha_{GB}} + \frac{1}{4} \kappa^2 \phi^2 - \dot{B} - \frac{\kappa^2 \phi^4}{\sigma \beta} \Big|_{hc}^f, \quad (87)$$

where

$$\dot{B} = 32 \frac{\kappa^6 \phi^6 e^{\kappa\phi} - 6\kappa^5 \phi^5 e^{\kappa\phi} + 30\kappa^4 \phi^4 e^{\kappa\phi} - 120\kappa^3 \phi^3 e^{\kappa\phi} + 360\kappa^2 \phi^2 e^{\kappa\phi} - 720\kappa\phi e^{\kappa\phi} + 720e^{\kappa\phi}}{\kappa^6 \sigma \beta^2 R_{GB} \alpha_{GB}}. \quad (88)$$

The evolution of the tensor to scalar ratio versus the spectral index is shown with the solid lines in the left panel of figure 1. For $\mathcal{V}(\phi) \sim e^{-\kappa\phi}$ and for $N = 50$, the model is inside the joint 95% CL of the Planck+WMAP9+BAO data if $1.14 \times 10^{-5} \leq \alpha_{GB} \leq 4.5 \times 10^{-3}$. For $N = 60$ the constraint on the Gauss-Bonnet coupling parameter is as $1.4 \times 10^{-5} \leq \alpha_{GB} \leq 4.4 \times 10^{-3}$. In the right panel of figure 1 we see the evolution of the amplitude of the non-Gaussianity in the orthogonal configuration versus the equilateral configuration in the background of 68%, 95% and 99% CL of the Planck+WMAP9+BAO data. For $\mathcal{V}(\phi) \sim e^{-\kappa\phi}$, the model is inside the joint 95% CL of the Planck+WMAP9+BAO data if $1.37 \times 10^{-4} \leq \alpha_{GB} \leq 4.61 \times 10^{-3}$ for $N = 50$ and $1.2 \times 10^{-4} \leq \alpha_{GB} \leq 4.581 \times 10^{-3}$ for $N = 60$. In this case, the model lies inside the 99% CL of the Planck+WMAP9+BAO data if $1.03 \times 10^{-4} < \alpha_{GB} < 4.9 \times 10^{-3}$ for $N = 50$ and $1 \times 10^{-4} \leq \alpha_{GB} \leq 5.21 \times 10^{-3}$ for $N = 60$.

5.1.2 $V(\phi) = \frac{\sigma}{4} \phi^4$

Now, we consider a quartic potential and similar to the previous subsection, we adopt three functions for $\mathcal{V}(\phi)$ as $\mathcal{V}(\phi) \sim \phi^2$, ϕ^4 and $e^{-\kappa\phi}$. At first, we solve the integral of equation (22) for $\mathcal{V}(\phi) \sim \phi^2$ and the result is

$$N = -\frac{3}{4} \frac{\kappa^2 \sigma \beta^2 \alpha_{GB} R_{GB} \ln(\sigma \phi^2 \beta + 8\phi^2 + 2\alpha_{GB} R_{GB} \beta)}{(3\sigma\beta + 24)(\sigma\beta + 8)} + 24 \frac{\kappa^6 \sigma \beta^3 \alpha_{GB}^4 R_{GB}^2 \dot{C}}{8\kappa^2 \alpha_{GB} \sigma \beta + 64\kappa^2 \alpha_{GB}} + 3 \frac{\kappa^4 \sigma \beta^2 \alpha_{GB}^2 R_{GB} \ln(-3\beta + 8\kappa^2 \beta \phi^4 \sigma \beta + 64\kappa^2 \alpha_{GB} \phi^4 + 16\kappa^2 \alpha_{GB}^2 \phi^2 R_{GB} \beta)}{(3\sigma\beta + 24)(8\kappa^2 \alpha_{GB} \sigma \beta + 64\kappa^2 \alpha_{GB})} + \frac{9}{16} \kappa^2 \sigma \beta^2 \dot{C} \Big|_{hc}^f, \quad (89)$$

where

$$\dot{C} = \frac{\arctan \left(\frac{1}{4} \frac{2(8\kappa^2 \alpha_{GB} \sigma \beta + 64\kappa^2 \alpha_{GB}) \phi^2 + 16\kappa^2 \alpha_{GB}^2 R_{GB} \beta}{\sqrt{6\kappa^2 \sigma \beta^2 \alpha_{GB} + 48\alpha_{GB} \beta \kappa^2 + 16\kappa^4 \alpha_{GB}^4 R_{GB}^2 \beta^2}} \right)}{(3\sigma\beta + 24) \sqrt{6\kappa^2 \sigma \beta^2 \alpha_{GB} + 48\alpha_{GB} \beta \kappa^2 + 16\kappa^4 \alpha_{GB}^4 R_{GB}^2 \beta^2}}, \quad (90)$$

By obtaining ϕ_{hc} and substituting it into equations (48) and (53), we plot the evolution of the tensor to scalar ratio versus the spectral index. The result is shown in the left panel of figure 2. We have found that for $\mathcal{V}(\phi) \sim \phi^2$, the model is compatible with the joint 95% CL of the Planck+WMAP9+BAO data if $1.5 \times 10^{-4} \leq \alpha_{GB} < 6.2 \times 10^{-3}$ and $1.71 \times 10^{-4} < \alpha_{GB} < 6.34 \times 10^{-3}$ for $N = 50$ and $N = 60$ respectively. The evolution of the amplitude of the non-Gaussianity in the orthogonal configuration versus the equilateral configuration in the background of 68%, 95% and 99% CL of the Planck+WMAP9+BAO data is shown in the right panel of figure 2. For $\mathcal{V}(\phi) \sim \phi^2$ and for $N = 50$, the model lies well inside the joint 95% CL of the Planck+WMAP9+BAO data if $1.43 \times 10^{-4} \leq \alpha_{GB} < 5.38 \times 10^{-3}$. Also, for $N = 60$ it is compatible with observation, if $1.6 \times 10^{-4} < \alpha_{GB} < 6.014 \times 10^{-3}$. In this case, for $N = 50$ and $N = 60$, the model lies within 99% CL of the Planck+WMAP9+BAO data if $1.3 \times 10^{-4} \leq \alpha_{GB} < 5.8 \times 10^{-3}$ and $1.52 \times 10^{-4} < \alpha_{GB} < 6.4 \times 10^{-3}$ respectively.

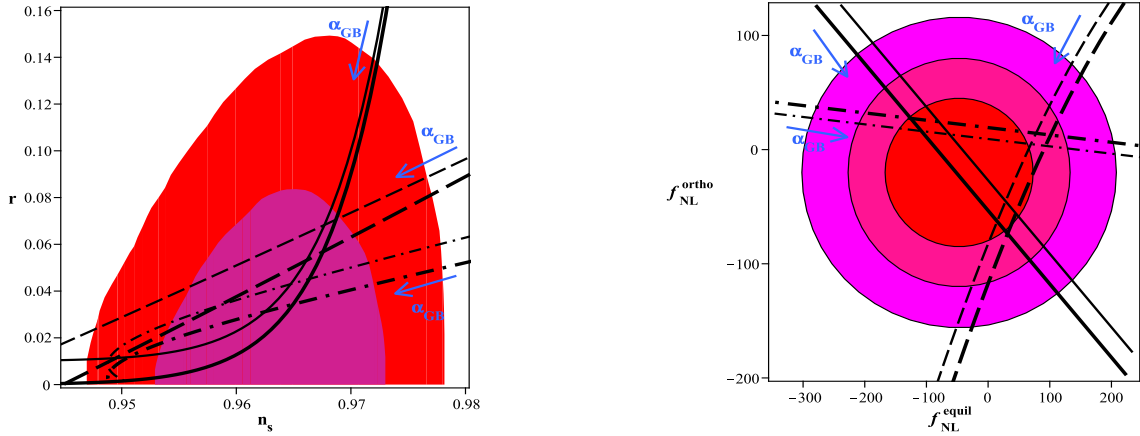


Figure 2: Evolution of the tensor to scalar ratio versus the spectral index (left panel) and the amplitude of the non-Gaussianity in the orthogonal configuration versus the equilateral configuration (right panel), for the case with $f(\phi) = \beta\phi^{-4}$ and with a quartic potential, in the background of Planck+WMAP9+BAO data.

The result of solving the integral of equation (22) with $\mathcal{V}(\phi) \sim \phi^4$ is given by

$$N = \frac{\kappa^2 \sigma \beta^2 3^{\frac{5}{6}} (32)^{\frac{2}{3}} \arctan \left(\frac{1}{3} \sqrt{3} \left(\frac{2}{3} \frac{3^{\frac{2}{3}} \sqrt[3]{32} \phi^2}{\sqrt[3]{D}} + 1 \right) \right) - \kappa^2 \sigma f^2 \sqrt[3]{3} (32)^{\frac{2}{3}} \ln \left(\phi^2 - \frac{1}{32} \sqrt[3]{3} (32)^{\frac{2}{3}} \sqrt[3]{D} \right)}{12 \dot{D}^{\frac{5}{3}}} + \frac{1}{24} \frac{\kappa^2 \sigma \beta^2 \sqrt[3]{3} (32)^{\frac{2}{3}} \ln \left(\phi^4 + \frac{1}{32} \phi^2 \sqrt[3]{3} (32)^{\frac{2}{3}} \sqrt[3]{D} + \frac{1}{32} 3^{\frac{2}{3}} \sqrt[3]{32} \dot{D}^{\frac{2}{3}} \right)}{\dot{D} \dot{D}^{2/3}} \bigg|_{hc}^f, \quad (91)$$

where

$$\dot{D} = \frac{\beta}{\kappa^2 \alpha_{GB} (\sigma \beta + 4 + 2 \alpha_{GB} R_{GB} \beta)} \quad (92)$$

For this case, the evolution of the tensor to scalar ratio versus the scalar spectral index is shown with dash-dotted lines in the left panel of figure 2. For $\mathcal{V}(\phi) \sim \phi^4$ and for $N = 50$, the model lies inside the joint 95% CL of the Planck+WMAP9+BAO data if $1.3 \times 10^{-5} < \alpha_{GB} < 8.6 \times 10^{-4}$.

Also, for $N = 60$ the model is compatible with observation if $1.38 \times 10^{-5} < \alpha_{GB} < 8.44 \times 10^{-4}$. The evolution of the f^{ortho} versus f^{equil} is shown in the right panel of figure 2. In studying the non-Gaussianity, it is obtained that, with this function, the model with $1.65 \times 10^{-5} < \alpha_{GB} \leq 8.471 \times 10^{-4}$, and with $1.8 \times 10^{-5} < \alpha_{GB} < 8.479 \times 10^{-4}$ for $N = 60$ lies inside the 95% CL of the Planck+WMAP9+BAO data. Also, comparison with the 99% CL of the Planck+WMAP9+BAO data shows that $1.47 \times 10^{-5} < \alpha_{GB} < 8.77 \times 10^{-4}$ for $N = 50$, and $1.5 \times 10^{-5} < \alpha_{GB} < 8.8 \times 10^{-4}$ for $N = 60$.

By adopting $\mathcal{V}(\phi) \sim e^{-\kappa\phi}$, solving the integral leads to

$$\begin{aligned}
N = & \frac{1}{8} \frac{\sigma \kappa^2 \phi^2 \beta}{\sigma \beta + 8} + \frac{1}{3} \frac{\sigma \alpha_{GB} (24 + 24\kappa\phi + 12\kappa^2 \phi^2 + 4\kappa^3 \phi^3 + \kappa^4 \phi^4)}{e^{\kappa\phi}} \\
& + \frac{1}{4} \sigma \beta \left(\frac{\sigma (\kappa^4 \phi^4 e^{\kappa\phi} - 4\kappa^3 \phi^3 e^{\kappa\phi} + 12\kappa^2 \phi^2 e^{\kappa\phi} - 24\kappa \phi e^{\kappa\phi} + 24 e^{\kappa\phi})}{\kappa^4 \alpha_{GB} R_{GB}} \right. \\
& \left. + 8 \frac{\kappa^4 \phi^4 e^{\kappa\phi} - 4\kappa^3 \phi^3 e^{\kappa\phi} + 12\kappa^2 \phi^2 e^{\kappa\phi} - 24\kappa \phi e^{\kappa\phi} + 24 e^{\kappa\phi}}{\kappa^4 \alpha_{GB} R_{GB} \beta} + \frac{1}{2} \kappa^2 \phi^2 \right) (\sigma \beta + 8)^{-1} \Big|_{hc}^f, \quad (93)
\end{aligned}$$

The solid lines in the left panel of figure 2 show the evolution of r versus n_s . We have found that, for $\mathcal{V}(\phi) \sim e^{-\kappa\phi}$ and for $N = 50$, the model is well inside the joint 95% CL of the Planck+WMAP9+BAO data if $1.96 \times 10^{-3} < \alpha_{GB} < 8.21 \times 10^{-3}$. For $N = 60$, we find the constraint on the Gauss-Bonnet coupling parameter as $1.85 \times 10^{-3} < \alpha_{GB} \leq 8.141 \times 10^{-3}$. Also the solid lines in the right panel of figure 2 show the evolution of f^{ortho} versus f^{equil} for $\mathcal{V}(\phi) \sim e^{-\kappa\phi}$ in the background of 68%, 95% and 99% CL of the Planck+WMAP9+BAO data. With this function, the model is compatible with the joint 95% CL of the Planck+WMAP9+BAO data if $2.05 \times 10^{-3} \leq \alpha_{GB} < 7.1 \times 10^{-3}$ for $N = 50$ and $1.95 \times 10^{-3} < \alpha_{GB} \leq 7.66 \times 10^{-3}$ for $N = 60$. Also, it is compatible with the joint 99% CL of the Planck+WMAP9+BAO data if $1.46 \times 10^{-3} < \alpha_{GB} < 8.73 \times 10^{-3}$ for $N = 50$ and $1.715 \times 10^{-3} \leq \alpha_{GB} \leq 7.9 \times 10^{-3}$ for $N = 60$.

5.1.3 $V(\phi) = \sigma e^{-\kappa\phi}$

The third potential that we consider here, is an exponentially type potential. With this potential, we solve the integral of equation (22) for $\mathcal{V}(\phi) \sim \phi^2$ to obtain

$$N = \frac{\sigma \kappa^2 \left(-\frac{8}{3} \alpha_{GB} - \frac{8}{3} \alpha_{GB} \kappa \phi \right)}{e^{\kappa\phi}} + \phi + 8 \frac{\kappa^3 \phi^3 - 3\kappa^2 \phi^2 + 6\kappa \phi - 6}{e^{-\kappa\phi} \kappa^4 \sigma \beta} + 2 \frac{\alpha_{GB} R_{GB} (\kappa \phi e^{\kappa\phi} - e^{\kappa\phi})}{\sigma \kappa^2} \Big|_{hc}^f. \quad (94)$$

We find ϕ_{hc} from this equation and substitute it into the equations (48) and (53) to obtain the evolution of n_s and r . One can see the evolution of the tensor to scalar ratio versus the scalar spectral index in the left panel of figure 3 (the dashed lines). With $\mathcal{V}(\phi) \sim \phi^2$, the model is compatible with the joint 95% CL of the Planck+WMAP9+BAO data if $8 \times 10^{-5} < \alpha_{GB} < 3.3 \times 10^{-4}$ and $4.8 \times 10^{-4} < \alpha_{GB} < 1.73 \times 10^{-3}$ for $N = 50$ and $8.36 \times 10^{-5} < \alpha_{GB} < 3.84 \times 10^{-4}$ and $5.5 \times 10^{-4} < \alpha_{GB} < 1.84 \times 10^{-3}$ for $N = 60$. The evolution of the amplitude of the non-Gaussianity in the orthogonal configuration versus the equilateral configuration in the background of 68%, 95% and 99% CL of the Planck+WMAP9+BAO data is shown in the right panel of the figure 3. In exploring

the amplitude of non-Gaussianity we find that the model for $N = 50$ lies inside the joint 95% CL of the Planck+WMAP9+BAO data if $8.65 \times 10^{-5} < \alpha_{GB} \leq 1.643 \times 10^{-3}$. Also, the model for $N = 60$ lies inside the joint 95% CL of the Planck+WMAP9+BAO data if $7.9 \times 10^{-5} < \alpha_{GB} < 1.5 \times 10^{-3}$. In this case, for $N = 50$ and $N = 60$, the model lies within 99% CL of the Planck+WMAP9+BAO data if $8 \times 10^{-5} < \alpha_{GB} < 1.73 \times 10^{-3}$ and $7.62 \times 10^{-5} < \alpha_{GB} < 1.74 \times 10^{-3}$ respectively.

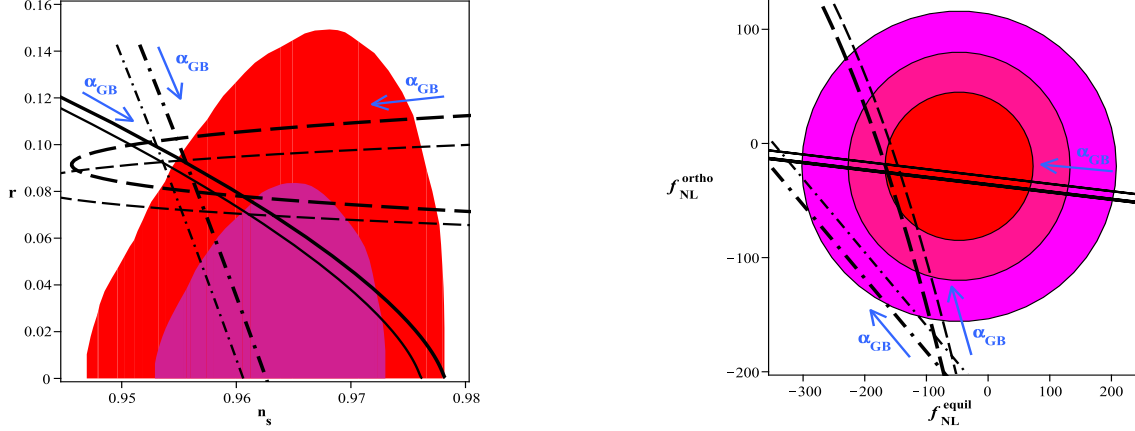


Figure 3: Evolution of the tensor to scalar ratio versus the spectral index (left panel) and the amplitude of the non-Gaussianity in the orthogonal configuration versus the equilateral configuration (right panel), for the case with $f(\phi) = \beta\phi^{-4}$ and with an exponential potential, in the background of Planck+WMAP9+BAO data.

The following equation is the result of solving equation (22) with $\mathcal{V}(\phi) \sim \phi^4$

$$N = \frac{16}{3} \frac{\sigma \alpha_{GB} (6 + 6\kappa\phi + 3\kappa^2\phi^2 + \kappa^3\phi^3)}{e^{\kappa\phi}} + \phi + 8 \frac{\kappa^3\phi^3 e^{\kappa\phi} - 3\kappa^2\phi^2 e^{\kappa\phi} + 6\kappa\phi e^{\kappa\phi} - 6e^{\kappa\phi}}{\kappa^4\sigma\beta} + 4 \frac{\alpha_{GB} R_{GB} (\kappa^3\phi^3 e^{\kappa\phi} - 3\kappa^2\phi^2 e^{\kappa\phi} + 6\kappa\phi e^{\kappa\phi} - 6e^{\kappa\phi})}{\kappa^4\sigma} \Big|_{hc}^f, \quad (95)$$

One can see the evolution of r versus n_s in the left panel of figure 3 (the dot-dashed lines). For $\mathcal{V}(\phi) \sim \phi^4$ and for $N = 50$, the model lies inside the joint 95% CL of the Planck+WMAP9+BAO data if $7.5 \times 10^{-5} < \alpha_{GB} < 6 \times 10^{-3}$. Also, for $N = 60$ the model is compatible with observation, if $7.66 \times 10^{-5} < \alpha_{GB} < 6.33 \times 10^{-3}$. The numerical study of the non-Gaussianity also, gives some constraints on the α_{GB} (see the dot-dashed lines in the right panel of figure 3). With $\mathcal{V}(\phi) \sim \phi^4$, the model for both $N = 50$ and $N = 60$ lies outside the 95% CL of the Planck+WMAP9+BAO data. But, it is compatible with the 99% CL of the Planck+WMAP9+BAO data if $7.38 \times 10^{-5} < \alpha_{GB} \leq 5.16 \times 10^{-3}$ for $N = 50$, and $5.66 \times 10^{-5} < \alpha_{GB} < 5.4 \times 10^{-3}$ for $N = 60$.

Finally we consider an exponential function for \mathcal{V} as $\mathcal{V}(\phi) \sim e^{-\kappa\phi}$ and solve the integral. We obtain

$$N = \frac{2}{3} \frac{\kappa^4 \alpha_{GB} \sigma}{e^{2\kappa\phi}} - \phi - 8 \frac{\kappa^3\phi^3 e^{\kappa\phi} - 3\kappa^2\phi^2 e^{\kappa\phi} + 6\kappa\phi e^{\kappa\phi} - 6e^{\kappa\phi}}{\sigma \kappa^4 \beta} + \frac{\kappa \alpha_{GB} R_{GB} \phi}{\sigma} \Big|_{hc}^f. \quad (96)$$

Table 1: The ranges of α_{GB} for which the values of the inflationary parameters r and n_s are compatible with the joint 95% CL of the Planck+WMAP9+BAO data for $f = \beta\phi^{-4}$

V	N	$\mathcal{V}(\phi) \sim \phi^2$	$\mathcal{V}(\phi) \sim \phi^4$	$\mathcal{V}(\phi) \sim e^{-\kappa\phi}$
$\frac{\sigma}{2}\phi^2$	$N = 50$	$3 \times 10^{-4} \leq \alpha_{GB} < 4.2 \times 10^{-3}$	$6 \times 10^{-4} < \alpha_{GB} < 2.44 \times 10^{-3}$	$1.14 \times 10^{-5} \leq \alpha_{GB} \leq 4.5 \times 10^{-3}$
$\frac{\sigma}{2}\phi^2$	$N = 60$	$2.9 \times 10^{-4} < \alpha_{GB} < 3.65 \times 10^{-3}$	$6.23 \times 10^{-4} < \alpha_{GB} < 2.524 \times 10^{-3}$	$1.4 \times 10^{-5} \leq \alpha_{GB} \leq 4.4 \times 10^{-3}$
$\frac{\sigma}{4}\phi^4$	$N = 50$	$1.5 \times 10^{-4} \leq \alpha_{GB} < 6.2 \times 10^{-3}$	$1.3 \times 10^{-5} \leq \alpha_{GB} < 8.6 \times 10^{-4}$	$1.96 \times 10^{-3} \leq \alpha_{GB} < 8.21 \times 10^{-3}$
$\frac{\sigma}{4}\phi^4$	$N = 60$	$1.71 \times 10^{-4} \leq \alpha_{GB} < 6.34 \times 10^{-3}$	$1.38 \times 10^{-5} \leq \alpha_{GB} < 8.44 \times 10^{-4}$	$1.85 \times 10^{-3} \leq \alpha_{GB} < 8.141 \times 10^{-3}$
$\sigma e^{-\kappa\phi}$	$N = 50$	$8 \times 10^{-5} \leq \alpha_{GB} < 3.3 \times 10^{-4}$ $4.8 \times 10^{-4} \leq \alpha_{GB} < 1.73 \times 10^{-3}$	$7.5 \times 10^{-5} \leq \alpha_{GB} < 6 \times 10^{-3}$	$3.76 \times 10^{-4} \leq \alpha_{GB} < 7.77 \times 10^{-3}$
$\sigma e^{-\kappa\phi}$	$N = 60$	$8.36 \times 10^{-5} \leq \alpha_{GB} < 3.84 \times 10^{-4}$ $5.5 \times 10^{-4} \leq \alpha_{GB} < 1.84 \times 10^{-3}$	$7.66 \times 10^{-5} \leq \alpha_{GB} < 6.33 \times 10^{-3}$	$3.64 \times 10^{-4} \leq \alpha_{GB} < 7.68 \times 10^{-3}$

Table 2: The ranges of α_{GB} for which the values of the inflationary parameters f^{ortho} and f^{equil} are compatible with the joint 99% CL of the Planck+WMAP9+BAO data for $f = \beta\phi^{-4}$

V	N	$\mathcal{V}(\phi) \sim \phi^2$	$\mathcal{V}(\phi) \sim \phi^4$	$\mathcal{V}(\phi) \sim e^{-\kappa\phi}$
$\frac{\sigma}{2}\phi^2$	$N = 50$	$2.8 \times 10^{-4} < \alpha_{GB} < 4.14 \times 10^{-3}$	$5.2 \times 10^{-4} < \alpha_{GB} \leq 3 \times 10^{-3}$	$1.03 \times 10^{-4} < \alpha_{GB} < 4.9 \times 10^{-3}$
$\frac{\sigma}{2}\phi^2$	$N = 60$	$2.71 \times 10^{-4} \leq \alpha_{GB} \leq 4.22 \times 10^{-3}$	$5.5 \times 10^{-4} < \alpha_{GB} < 3.02 \times 10^{-3}$	$1 \times 10^{-4} \leq \alpha_{GB} < 5.21 \times 10^{-3}$
$\frac{\sigma}{4}\phi^4$	$N = 50$	$1.3 \times 10^{-4} \leq \alpha_{GB} < 5.8 \times 10^{-3}$	$1.47 \times 10^{-5} < \alpha_{GB} < 8.77 \times 10^{-4}$	$1.46 \times 10^{-3} < \alpha_{GB} < 8.73 \times 10^{-3}$
$\frac{\sigma}{4}\phi^4$	$N = 60$	$1.52 \times 10^{-4} < \alpha_{GB} < 6.4 \times 10^{-3}$	$1.5 \times 10^{-5} < \alpha_{GB} < 8.8 \times 10^{-4}$	$1.715 \times 10^{-3} \leq \alpha_{GB} \leq 7.9 \times 10^{-3}$
$\sigma e^{-\kappa\phi}$	$N = 50$	$8 \times 10^{-5} < \alpha_{GB} < 1.73 \times 10^{-3}$	$7.38 \times 10^{-5} < \alpha_{GB} \leq 5.16 \times 10^{-3}$	$3.261 \times 10^{-4} \leq \alpha_{GB} < 7.29 \times 10^{-3}$
$\sigma e^{-\kappa\phi}$	$N = 60$	$7.62 \times 10^{-5} < \alpha_{GB} < 1.74 \times 10^{-3}$	$5.66 \times 10^{-5} < \alpha_{GB} < 5.4 \times 10^{-3}$	$3.13 \times 10^{-4} < \alpha_{GB} < 7.5 \times 10^{-3}$

The solid lines in the left panel of figure 3 are corresponding to $\mathcal{V}(\phi) \sim e^{-\kappa\phi}$. With an exponential potential and with $\mathcal{V}(\phi) \sim e^{-\kappa\phi}$, the model is well inside the joint 95% CL of the Planck+WMAP9+BAO data for $N = 50$ and $N = 60$, if $3.76 \times 10^{-4} < \alpha_{GB} < 7.77 \times 10^{-3}$ and $3.64 \times 10^{-4} < \alpha_{GB} < 7.68 \times 10^{-3}$ respectively. The solid lines in the right panel of figure 3 are corresponding to $\mathcal{V}(\phi) \sim e^{-\kappa\phi}$. We have found that with an exponential potential and with $\mathcal{V}(\phi) \sim e^{-\kappa\phi}$, the model is compatible with the joint 95% CL of the Planck+WMAP9+BAO data if $3.46 \times 10^{-4} < \alpha_{GB} < 7.18 \times 10^{-3}$ for $N = 50$ and $3.4 \times 10^{-4} < \alpha_{GB} < 7.26 \times 10^{-3}$ for $N = 60$. Also, a comparison with the joint 99% CL of the Planck+WMAP9+BAO data shows that this model is compatible with observational data if $3.261 \times 10^{-4} \leq \alpha_{GB} < 7.29 \times 10^{-3}$ for $N = 50$ and $3.13 \times 10^{-4} < \alpha_{GB} < 7.5 \times 10^{-3}$ for $N = 60$. The results of these arguments are summarized in tables 1 and 2.

5.2 $f(\phi) = \beta e^{\kappa\phi}$

The second function we choose for $f(\phi)$ is an exponential function. For this type of $f(\phi)$, similar to the previous part we consider three types of potentials: quadratic, quartic and exponential potential. Then, we obtain some constraints on the model by comparing the main inflationary parameters of the model with the Planck+WMAP9+ BAO data.

5.2.1 $V(\phi) = \frac{\sigma}{2}\phi^2$

With this potential, we consider three functions $\mathcal{V}(\phi) \sim \phi^2$, ϕ^4 and $e^{-\kappa\phi}$ and we solve the integral of equation (22). For $\mathcal{V}(\phi) \sim \phi^2$ we obtain

$$N = \frac{1}{2} \frac{\sigma\kappa^2 \left(\frac{1}{4} \left(8\sigma\kappa^2\alpha_{GB} + 16\kappa^2\alpha_{GB}^2 R_{GB} \right) \phi^4 + \frac{3}{2}\phi^2 \right)}{6\alpha_{GB}R_{GB} + 3\sigma} + \frac{1}{4} \frac{\sigma^2\beta \left(\kappa^2\phi^2 e^{\kappa\phi} - 2\kappa\phi e^{\kappa\phi} + 2e^{\kappa\phi} \right)}{\kappa^2 (2\alpha_{GB}R_{GB} + \sigma)} + \frac{1}{4} \frac{\sigma\kappa^2\phi^2}{2\alpha_{GB}R_{GB} + \sigma} + \frac{\sigma\alpha_{GB}R_{GB}\beta \left(\kappa^2\phi^2 e^{\kappa\phi} - 2\kappa\phi e^{\kappa\phi} + 2e^{\kappa\phi} \right)}{2\kappa^2 (2\alpha_{GB}R_{GB} + \sigma)} \Big|_{hc}, \quad (97)$$

By finding ϕ_{hc} from this equation and then using equations (48) and (53), we plot the evolution of the tensor to scalar ratio versus the spectral index (left panel of figure 4). As we see from this figure, for some values of α_{GB} , the model is compatible with observational data. With $\mathcal{V}(\phi) \sim \phi^2$ and for $N = 50$, the model is observationally viable if $4.63 \times 10^{-4} < \alpha_{GB} < 6.54 \times 10^{-3}$. For $N = 60$ the model is compatible with observational data if $4.47 \times 10^{-4} < \alpha_{GB} < 6.4 \times 10^{-3}$. The right panel of figure 4 shows the evolution of the amplitude of the non-Gaussianity in the orthogonal configuration versus the equilateral configuration in the background of 68%, 95% and 99% CL of the Planck+WMAP9+BAO data. By adopting $\mathcal{V}(\phi) \sim \phi^2$, this model for $N = 50$ is compatible with the joint 95% CL of the Planck+WMAP9+BAO data if $4.713 \times 10^{-4} \leq \alpha_{GB} < 6.7 \times 10^{-3}$. Also, for $N = 60$ it is compatible with observation if $4.55 \times 10^{-4} < \alpha_{GB} < 6.61 \times 10^{-3}$. With this type of \mathcal{V} , the model is well inside the 99% CL of the Planck+WMAP9+BAO data if $4.66 \times 10^{-4} < \alpha_{GB} \leq 6.774 \times 10^{-3}$ for $N = 50$ and $4.41 \times 10^{-4} < \alpha_{GB} < 6.73 \times 10^{-3}$ for $N = 60$.

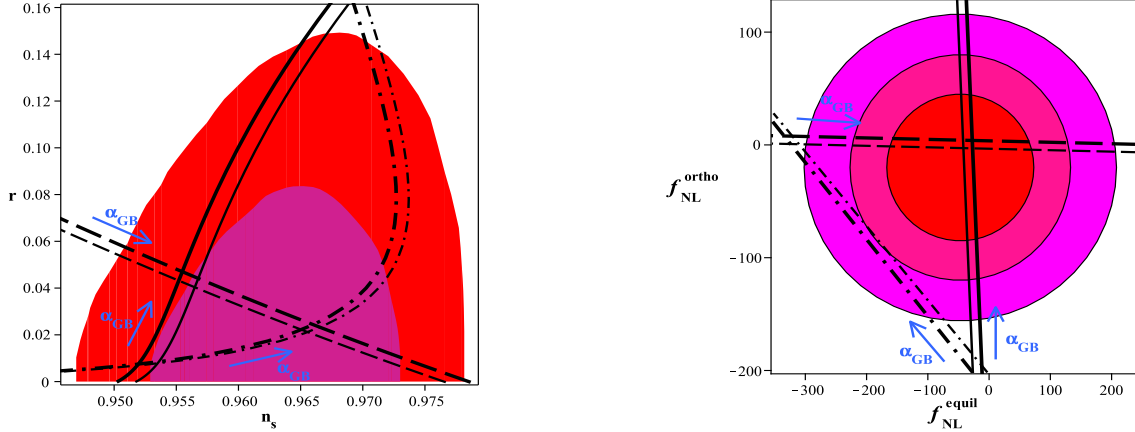


Figure 4: Evolution of the tensor to scalar ratio versus the spectral index (left panel) and the amplitude of the non-Gaussianity in the orthogonal configuration versus the equilateral configuration (right panel), for the case with $f(\phi) = \beta e^{\kappa\phi}$ and with a quadratic potential, in the background of the Planck+WMAP9+BAO data. The figure has been plotted for $N = 50$ (the thinner line) and 70 (the thicker line). The solid lines are corresponding to $\mathcal{V}(\phi) \sim e^{-\kappa\phi}$, the dashed lines are corresponding to $\mathcal{V}(\phi) \sim \phi^2$ and the dash-dotted lines are corresponding to $\mathcal{V}(\phi) \sim \phi^4$. For both values of N , a model with a non-minimal coupling between the Gauss-Bonnet term and the DBI field, in some ranges of α_{GB} is compatible with observational data.

By solving the integral of equation (22) with $\mathcal{V}(\phi) \sim \phi^4$, we obtain the following expression

$$N = \frac{4}{9}\sigma\kappa^4\alpha_{GB}\phi^6 + \frac{1}{16}\frac{\sigma\kappa^2\ln(\sigma + 4\alpha_{GB}\phi^2R_{GB})}{\alpha_{GB}R_{GB}} + \frac{1}{16}\frac{\kappa^2\ln(\sigma\kappa^2 + 4\alpha_{GB}\phi^2R_{GB}\kappa^2)}{\sigma\alpha_{GB}R_{GB}} \\ + \frac{1}{2}\frac{\beta e^{\kappa\phi}}{\sigma\kappa^2} - \frac{1}{2}\frac{\beta e^{\kappa\phi}\phi}{\sigma\kappa} + \frac{1}{4}\frac{\beta e^{\kappa\phi}\phi^2}{\sigma} \Bigg|_{hc}^f. \quad (98)$$

With a quadratic potential, the model for $N = 50$ is inside the joint 95% CL of the Planck+WMAP9+BAO data if $8.11 \times 10^{-5} < \alpha_{GB} < 3.42 \times 10^{-2}$. Also for $N = 60$ the condition is $8 \times 10^{-5} < \alpha_{GB} < 3.38 \times 10^{-2}$ (see the left panel of figure 4). By treating the amplitude of the non-Gaussianity (the right panel of figure 4) we find that, similar to the case with $f(\phi) = \beta\phi^{-4}$, this model with a quadratic potential and $\mathcal{V}(\phi) \sim \phi^4$, both for $N = 50$ and $N = 60$ is outside the 95% CL of the Planck+WMAP9+BAO data. However, for $N = 50$, the model with $3.1 \times 10^{-4} < \alpha_{GB} < 4.02 \times 10^{-3}$ and for $N = 60$, the model with $3.18 \times 10^{-4} < \alpha_{GB} < 4.15 \times 10^{-3}$ lies inside the 99% CL of the Planck+WMAP9+BAO data.

The result of solving the integral of equation (22) with $\mathcal{V}(\phi) \sim e^{-\kappa\phi}$ is as follows

$$N = \frac{1}{4}\kappa^2\phi^2 + \frac{1}{2}\frac{\sigma\kappa^2\left(\frac{8}{3}\alpha_{GB} + \frac{8}{3}\kappa\phi\alpha_{GB} + \frac{4}{3}\kappa^2\alpha_{GB}\phi^2\right)}{e^{\kappa\phi}} \\ - \frac{1}{4}(2 + \alpha_{GB}R_{GB}\beta)\left(\frac{1}{2}\frac{\sigma\beta(\kappa^2\phi^2e^{\kappa\phi} - 2\kappa\phi e^{\kappa\phi} + 2e^{\kappa\phi})}{\kappa^2} + \frac{1}{2}\kappa^2\phi^2 - \frac{1}{4}\kappa^2\alpha_{GB}\phi^2R_{GB}\beta\right) \Bigg|_{hc}^f. \quad (99)$$

The solid lines in the left pane of figure 4, that show the evolution of r versus n_s , are corresponding to $\mathcal{V}(\phi) \sim e^{-\kappa\phi}$. We have found that for $\mathcal{V}(\phi) \sim e^{-\kappa\phi}$ and for $N = 50$, the model is inside the joint 95% CL of the Planck+WMAP9+BAO data if $1.3 \times 10^{-4} < \alpha_{GB} < 9.03 \times 10^{-3}$. For $N = 60$, we have found that the constraint on the Gauss-Bonnet coupling parameter is as $1.41 \times 10^{-4} < \alpha_{GB} < 9.1 \times 10^{-3}$. Comparing the amplitude of the non-Gaussianity of this model with observational data (the right panel of figure 4) shows that, if we adopt $\mathcal{V}(\phi) \sim e^{-\kappa\phi}$, the model is well inside the joint 95% CL of the Planck+WMAP9+BAO data if $1.64 \times 10^{-4} < \alpha_{GB} \leq 8.781 \times 10^{-3}$ for $N = 50$ and $1.7 \times 10^{-4} < \alpha_{GB} < 8.87 \times 10^{-3}$ for $N = 60$. This model lies inside the 99% CL of the Planck+WMAP9+BAO data if $1.56 \times 10^{-4} < \alpha_{GB} < 8.9 \times 10^{-3}$ for $N = 50$ and $1.62 \times 10^{-4} < \alpha_{GB} < 9 \times 10^{-3}$ for $N = 60$.

5.2.2 $V(\phi) = \frac{\sigma}{4}\phi^4$

By considering a quartic potential and adopting three functions for $\mathcal{V}(\phi)$, we solve the integral of equation (22). The result for $\mathcal{V}(\phi) \sim \phi^2$ is given by

$$N = \frac{1}{36}\frac{\kappa^2\left(4\sigma^2\phi^6\kappa^2\alpha_{GB} + \frac{9}{2}\sigma\phi^2\right)}{\sigma} - \frac{1}{4}\frac{\alpha_{GB}R_{GB}\kappa^2\ln(\sigma\phi^2 + 2\alpha_{GB}R_{GB})}{\sigma} + 3\frac{\beta e^{\kappa\phi}\sigma}{\kappa^4} - 3\frac{\beta e^{\kappa\phi}\phi\sigma}{\kappa^3} \\ + \frac{3}{2}\frac{\beta e^{\kappa\phi}\phi^2\sigma}{\kappa^2} - \frac{1}{2}\frac{\beta e^{\kappa\phi}\phi^3\sigma}{\kappa} + \frac{1}{8}\sigma\beta e^{\kappa\phi}\phi^4 + \frac{1}{8}\kappa^2\phi^2 - \frac{1}{4}\frac{\kappa\alpha_{GB}R_{GB}\ln(\sigma\phi^2\kappa^2 + 2\alpha_{GB}R_{GB}\kappa^2)}{\sigma} \Bigg|_{hc}^f, \quad (100)$$

As usual, we obtain ϕ_{hc} , substitute it into equations (48) and (53) and then plot the evolution of the tensor to scalar ratio versus the spectral index (left panel of figure 5). With $\mathcal{V}(\phi) \sim \phi^2$, we find the

constraint on α_{GB} as $3 \times 10^{-3} < \alpha_{GB} < 4.5 \times 10^{-2}$ (for $N = 50$) and $3.08 \times 10^{-3} < \alpha_{GB} < 4.44 \times 10^{-2}$ (for $N = 60$). By comparing the non-Gaussianity of this model with observation (right panel of figure 5) we see that in this case the model for $N = 50$ lies well inside the joint 95% CL of the Planck+WMAP9+BAO data if $1.46 \times 10^{-3} < \alpha_{GB} \leq 4.143 \times 10^{-2}$. Also, for $N = 60$ it is compatible with observation if $1.16 \times 10^{-3} < \alpha_{GB} \leq 4.124 \times 10^{-2}$. In this case, for $N = 50$ and $N = 60$, the model lies within 99% CL of the Planck+WMAP9+BAO data if $1.3 \times 10^{-3} < \alpha_{GB} < 4.26 \times 10^{-2}$ and $1 \times 10^{-3} < \alpha_{GB} < 4.38 \times 10^{-2}$ respectively.

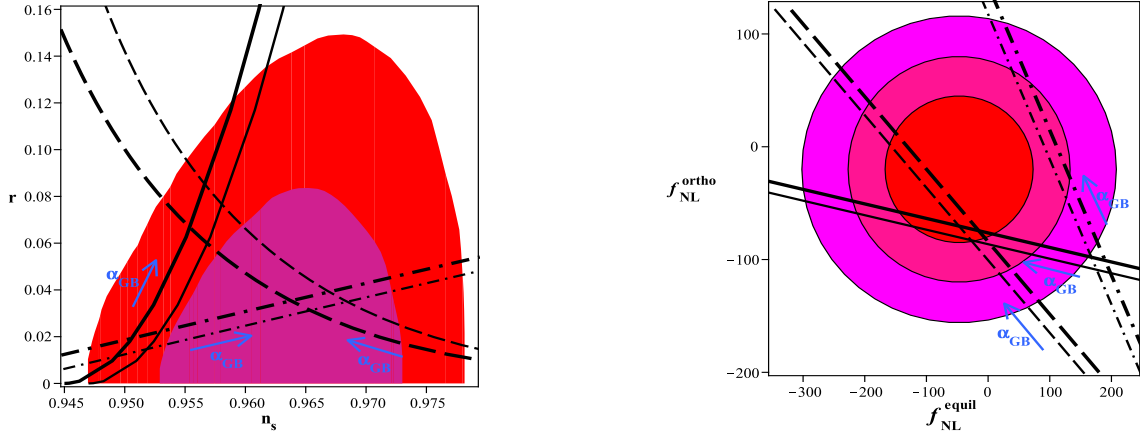


Figure 5: Evolution of the tensor to scalar ratio versus the spectral index (left panel) and the amplitude of the non-Gaussianity in the orthogonal configuration versus the equilateral configuration (right panel), for the case with $f(\phi) = \beta e^{\kappa\phi}$ and with a quartic potential, in the background of Planck+WMAP9+BAO data.

By adopting $\mathcal{V}(\phi) \sim \phi^4$, the integral (22) gives

$$\begin{aligned}
N = & \frac{1}{2} \frac{\sigma \kappa^2 \left(\frac{1}{8} (32\sigma \kappa^2 \alpha_{GB} + 64\alpha_{GB}^2 R_{GB} \kappa^2) \phi^8 + \frac{3}{2} \phi^2 \right)}{6\sigma + 12\alpha_{GB} R_{GB}} + \frac{1}{4} \frac{\sigma \phi^2}{(\sigma + 2\alpha_{GB} R_{GB}) \kappa^2} \\
& + \frac{1}{16} \frac{\sigma^3 \beta \left(\kappa^4 \phi^4 e^{\kappa\phi} - 4\kappa^3 \phi^3 e^{\kappa\phi} + 12\kappa^2 \phi^2 e^{\kappa\phi} - 24\kappa \phi e^{\kappa\phi} + 24e^{\kappa\phi} \right)}{(\sigma + 2\alpha_{GB} R_{GB}) \kappa^4} \\
& + \frac{1}{2} \frac{\sigma \alpha_{GB} R_{GB} \beta \left(\kappa^4 \phi^4 e^{\kappa\phi} - 4\kappa^3 \phi^3 e^{\kappa\phi} + 12\kappa^2 \phi^2 e^{\kappa\phi} - 24\kappa \phi e^{\kappa\phi} + 24e^{\kappa\phi} \right)}{(\sigma + 2\alpha_{GB} R_{GB}) \kappa^4} \Bigg|_{hc}, \quad (101)
\end{aligned}$$

The dot-dashed lines in the left panel of figure 5 show the evolution of r versus n_s with $\mathcal{V}(\phi) \sim \phi^4$. This model for $N = 50$ lies inside the joint 95% CL of the Planck+WMAP9+BAO data if $0.9 \times 10^{-4} < \alpha_{GB} < 8.5 \times 10^{-3}$. Also, for $N = 60$ the model is compatible with observation if $0.83 \times 10^{-4} < \alpha_{GB} < 8.38 \times 10^{-3}$. Other constraints on α_{GB} come from the study of the amplitude of the non-Gaussianity. A comparison with the 95% CL of the Planck+WMAP9+BAO data shows that with this type of \mathcal{V} , the model with $1.56 \times 10^{-4} < \alpha_{GB} < 7.89 \times 10^{-3}$, for $N = 50$, and with $1.3 \times 10^{-4} < \alpha_{GB} < 8.1 \times 10^{-3}$ for $N = 60$ is compatible with observation. This model is inside

the 99% CL of the Planck+WMAP9+BAO data if $1.43 \times 10^{-4} < \alpha_{GB} < 8.02 \times 10^{-3}$ for $N = 50$, and $1.15 \times 10^{-4} < \alpha_{GB} < 8.26 \times 10^{-3}$ for $N = 60$.

Similarly, the number of e-fold parameter with a quartic potential and with $\mathcal{V}(\phi) \sim e^{-\kappa\phi}$ becomes

$$N = \frac{1}{8}\phi^2\kappa^2 + \frac{1}{3}\frac{\sigma\alpha_{GB}(24 + 24\kappa\phi + 12\phi^2\kappa^2 + 4\kappa^3\phi^3 + \phi^4\kappa^4)}{e^{\kappa\phi}} - \frac{1}{8}(2 + \alpha_{GB}R_{GB}\beta) \times \left(-\frac{1}{2}\frac{\sigma\beta(\phi^4\kappa^4e^{\kappa\phi} - 4\kappa^3\phi^3e^{\kappa\phi} + 12\phi^2\kappa^2e^{\kappa\phi} - 24\kappa\phi e^{\kappa\phi} + 24e^{\kappa\phi})}{\kappa^4} + \frac{1}{2}\phi^2\kappa^2 + \frac{1}{4}\phi^2\kappa^2\alpha_{GB}R_{GB}\beta \right) \Bigg|_{hc}^f, \quad (102)$$

By studying the evolution of the tensor to scalar ratio versus the spectral index (the solid lines in the left panel of figure 5) we find that for $\mathcal{V}(\phi) \sim e^{-\kappa\phi}$ and for $N = 50$, the model is well inside the joint 95% CL of the Planck+WMAP9+BAO data if $6.86 \times 10^{-4} < \alpha_{GB} < 6.44 \times 10^{-3}$. For $N = 60$, we have found the constraint on the Gauss-Bonnet coupling parameter as $6.67 \times 10^{-4} < \alpha_{GB} < 6.31 \times 10^{-3}$. Also, studying the evolution of the amplitude of the non-Gaussianity in the orthogonal configuration versus the amplitude of the non-Gaussianity in the equilateral configuration (the solid lines in the right panel of figure 5) shows that with quartic potential and with $\mathcal{V}(\phi) \sim e^{-\kappa\phi}$, the model is compatible with the joint 95% CL of the Planck+WMAP9+BAO data if $6.71 \times 10^{-4} < \alpha_{GB} \leq 8.144 \times 10^{-3}$ for $N = 50$ and $6.64 \times 10^{-4} < \alpha_{GB} < 6.2 \times 10^{-3}$ for $N = 60$. Also, it is compatible with the joint 99% CL of the Planck+WMAP9+BAO data if $6.62 \times 10^{-4} < \alpha_{GB} < 8.3 \times 10^{-3}$ for $N = 50$ and $6.6 \times 10^{-4} < \alpha_{GB} \leq 6.265 \times 10^{-3}$ for $N = 60$.

5.2.3 $V(\phi) = \sigma e^{-\kappa\phi}$

The last potential which we consider, is an exponential type potential. By solving the integral of equation (22) with this type of potential and with $\mathcal{V}(\phi) \sim \phi^2$, we find

$$N = \frac{\sigma\kappa^2\left(-\frac{8}{3}\alpha_{GB} - \frac{8}{3}\kappa\alpha_{GB}\phi\right)}{e^{\kappa\phi}} + \sigma\kappa^2\beta\left(\phi - 2\frac{\phi}{\sigma\beta} + 2\frac{\alpha_{GB}R_{GB}(\kappa\phi e^{\kappa\phi} - e^{\kappa\phi})}{\kappa^3\sigma}\right) \Bigg|_{hc}^f, \quad (103)$$

By plotting the evolution of the tensor to scalar ratio versus the spectral index (the dashed lines in the left panel of figure 6) we can find new constraints on α_{GB} . With an exponential potential and with $\mathcal{V}(\phi) \sim \phi^2$, the model is compatible with observation if $6.1 \times 10^{-4} < \alpha_{GB} < 8.9 \times 10^{-3}$ for $N = 50$ and $5.97 \times 10^{-4} < \alpha_{GB} < 8.81 \times 10^{-3}$ for $N = 60$. Also by considering the amplitude of non-Gaussianity, we find other constraints on α_{GB} (see the dashed lines in the right panel of figure 6). In this case, the model for $N = 50$ lies inside the joint 95% CL of the Planck+WMAP9+BAO data if $6.44 \times 10^{-4} < \alpha_{GB} < 9.27 \times 10^{-3}$. Also, the model for $N = 60$ lies inside the joint 95% CL of the Planck+WMAP9+BAO data if $6.3 \times 10^{-4} < \alpha_{GB} < 9.02 \times 10^{-3}$. For $N = 50$ and $N = 60$, the model lies within 99% CL of the Planck+WMAP9+BAO data if $6.23 \times 10^{-4} < \alpha_{GB} < 9.36 \times 10^{-3}$ and $6.125 \times 10^{-4} \leq \alpha_{GB} \leq 9.141 \times 10^{-3}$ respectively.

If we take $\mathcal{V}(\phi) \sim \phi^4$, we find the following expression for the number of e-fold parameter

$$N = \phi - \frac{16}{3}\frac{\sigma\alpha_{GB}(6 + 6\kappa\phi + 3\kappa^2\phi^2 + \kappa^3\phi^3)}{e^{\kappa\phi}} + \frac{2\phi}{\sigma\beta} - \frac{4\alpha_{GB}R_{GB}(\kappa^3\phi^3 - 3\kappa^2\phi^2 + 6\kappa\phi - 6)}{e^{-\kappa\phi}\kappa^4\sigma} \Bigg|_{hc}^f, \quad (104)$$

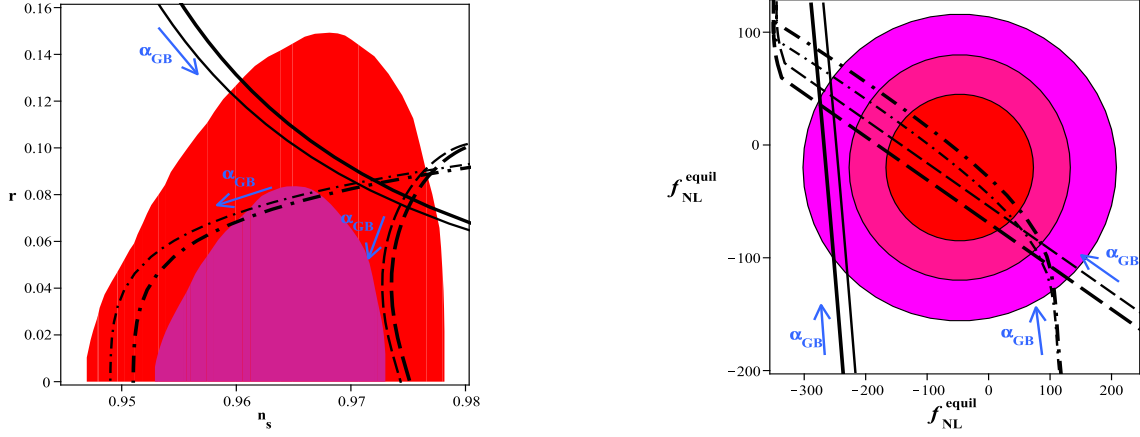


Figure 6: Evolution of the tensor to scalar ratio versus the spectral index (left panel) and the amplitude of the non-Gaussianity in the orthogonal configuration versus the equilateral configuration(right panel), for the case with $f(\phi) = \beta e^{\kappa\phi}$ and with an exponential potential, in the background of the Planck+WMAP9+BAO data.

With this type of \mathcal{V} , we plot r versus n_s (the dot-dashed lines in the left panel of figure 6). With $\mathcal{V}(\phi) \sim \phi^4$ and for $N = 50$, the model lies inside the joint 95% CL of the Planck+WMAP9+BAO data if $8.06 \times 10^{-5} < \alpha_{GB} < 7.4 \times 10^{-3}$. Also, for $N = 60$ the model is compatible with observation if $8 \times 10^{-5} < \alpha_{GB} < 7.33 \times 10^{-3}$. We also plot the evolution of f^{ortho} versus f^{equil} for $\mathcal{V}(\phi) \sim \phi^4$ (the dot-dashed lines in the right panel of figure 6). We find that this model lies inside the 95% CL of the Planck+WMAP9+BAO data if $8.11 \times 10^{-5} < \alpha_{GB} < 7.69 \times 10^{-3}$ for $N = 50$, and $8.06 \times 10^{-5} < \alpha_{GB} < 7.8 \times 10^{-3}$ for $N = 60$. Also, it is compatible with the 99% CL of the Planck+WMAP9+BAO data if $8.03 \times 10^{-5} < \alpha_{GB} < 7.76 \times 10^{-3}$ for $N = 50$, and $8 \times 10^{-5} < \alpha_{GB} < 7.87 \times 10^{-3}$ for $N = 60$.

Finally we solve the integral of equation (22) with $\mathcal{V}(\phi) \sim e^{-\kappa\phi}$ and find

$$N = -\frac{1}{2} \frac{\sigma\beta \ln \left(-3 \left(e^{\kappa\phi} \right)^2 \beta + 4\kappa^4 \alpha_{GB} \sigma\beta + 8\kappa^4 \alpha_{GB} + 4\kappa^4 \alpha_{GB}^2 R_{GB} \beta \right)}{\sigma\beta + 2 + \alpha_{GB} R_{GB} \beta} \Big|_{hc}^f, \quad (105)$$

The solid lines in the left panel of figure 6 show the tensor to scalar ratio versus the spectral index for $\mathcal{V}(\phi) \sim e^{-\kappa\phi}$. In this case the model lies inside the joint 95% CL of the Planck+WMAP9+BAO data for $N = 50$ and $N = 60$, if $3.73 \times 10^{-4} < \alpha_{GB} < 1.24 \times 10^{-2}$ and $3.69 \times 10^{-4} < \alpha_{GB} < 1.21 \times 10^{-2}$ respectively. Also, the solid lines in the left panel of figure 6 show the evolution of f^{ortho} versus f^{equil} with $\mathcal{V}(\phi) \sim e^{-\kappa\phi}$. This model with an exponential potential and with $\mathcal{V}(\phi) \sim e^{-\kappa\phi}$ is outside the joint 95% CL of the Planck+WMAP9+BAO data, both for $N = 50$ and $N = 60$. But, a comparison with the joint 99% CL of the Planck+WMAP9+BAO data shows that this model is compatible with observation if $4.3 \times 10^{-4} < \alpha_{GB} < 1.16 \times 10^{-2}$ for $N = 50$ and $4.24 \times 10^{-4} < \alpha_{GB} < 1.3 \times 10^{-2}$ for $N = 60$. The results of these arguments are summarized in tables 3 and 4.

Table 3: The ranges of α_{GB} for which the values of the inflationary parameters r and n_s are compatible with the joint 95% CL of the Planck+WMAP9+BAO data with $f = \beta e^{\kappa\phi}$.

V	N	$\mathcal{V}(\phi) \sim \phi^2$	$\mathcal{V}(\phi) \sim \phi^4$	$\mathcal{V}(\phi) \sim e^{-\kappa\phi}$
$\frac{\sigma}{2}\phi^2$	$N = 50$	$4.63 \times 10^{-4} < \alpha_{GB} < 6.54 \times 10^{-3}$	$8.11 \times 10^{-5} < \alpha_{GB} < 3.42 \times 10^{-2}$	$1.3 \times 10^{-4} < \alpha_{GB} < 9.03 \times 10^{-3}$
$\frac{\sigma}{2}\phi^2$	$N = 60$	$4.47 \times 10^{-4} < \alpha_{GB} < 6.4 \times 10^{-3}$	$8 \times 10^{-5} < \alpha_{GB} < 3.38 \times 10^{-2}$	$1.41 \times 10^{-4} < \alpha_{GB} < 9.1 \times 10^{-3}$
$\frac{\sigma}{4}\phi^4$	$N = 50$	$3 \times 10^{-3} < \alpha_{GB} < 4.5 \times 10^{-2}$	$0.9 \times 10^{-4} < \alpha_{GB} < 8.5 \times 10^{-3}$	$6.86 \times 10^{-4} < \alpha_{GB} < 6.44 \times 10^{-3}$
$\frac{\sigma}{4}\phi^4$	$N = 60$	$3.08 \times 10^{-3} < \alpha_{GB} < 4.44 \times 10^{-2}$	$0.83 \times 10^{-4} < \alpha_{GB} < 8.38 \times 10^{-3}$	$6.67 \times 10^{-4} < \alpha_{GB} < 6.31 \times 10^{-3}$
$\sigma e^{-\kappa\phi}$	$N = 50$	$6.1 \times 10^{-4} < \alpha_{GB} < 8.9 \times 10^{-3}$	$8.06 \times 10^{-5} < \alpha_{GB} < 7.4 \times 10^{-3}$	$3.73 \times 10^{-4} < \alpha_{GB} < 1.24 \times 10^{-2}$
$\sigma e^{-\kappa\phi}$	$N = 60$	$5.97 \times 10^{-4} < \alpha_{GB} < 8.81 \times 10^{-3}$	$8 \times 10^{-5} < \alpha_{GB} < 7.33 \times 10^{-3}$	$3.69 \times 10^{-4} < \alpha_{GB} < 1.21 \times 10^{-2}$

Table 4: The ranges of α_{GB} for which the values of the inflationary parameters f^{ortho} and f^{equil} are compatible with the joint 99% CL of the Planck+WMAP9+BAO data with $f = \beta e^{\kappa\phi}$.

V	N	$\mathcal{V}(\phi) \sim \phi^2$	$\mathcal{V}(\phi) \sim \phi^4$	$\mathcal{V}(\phi) \sim e^{-\kappa\phi}$
$\frac{\sigma}{2}\phi^2$	$N = 50$	$4.66 \times 10^{-4} < \alpha_{GB} \leq 6.774 \times 10^{-3}$	$3.1 \times 10^{-4} < \alpha_{GB} < 4.02 \times 10^{-3}$	$1.56 \times 10^{-4} < \alpha_{GB} < 8.9 \times 10^{-3}$
$\frac{\sigma}{2}\phi^2$	$N = 60$	$4.41 \times 10^{-4} < \alpha_{GB} < 6.73 \times 10^{-3}$	$3.18 \times 10^{-4} < \alpha_{GB} < 4.15 \times 10^{-3}$	$1.62 \times 10^{-4} < \alpha_{GB} < 9 \times 10^{-3}$
$\frac{\sigma}{4}\phi^4$	$N = 50$	$1.3 \times 10^{-3} < \alpha_{GB} < 4.26 \times 10^{-2}$	$1.43 \times 10^{-4} < \alpha_{GB} < 8.02 \times 10^{-3}$	$6.62 \times 10^{-4} < \alpha_{GB} < 8.3 \times 10^{-3}$
$\frac{\sigma}{4}\phi^4$	$N = 60$	$1 \times 10^{-3} < \alpha_{GB} < 4.38 \times 10^{-2}$	$1.15 \times 10^{-4} < \alpha_{GB} < 8.26 \times 10^{-3}$	$6.6 \times 10^{-4} < \alpha_{GB} \leq 6.265 \times 10^{-3}$
$\sigma e^{-\kappa\phi}$	$N = 50$	$6.23 \times 10^{-4} < \alpha_{GB} < 9.36 \times 10^{-3}$	$8.03 \times 10^{-5} < \alpha_{GB} < 7.76 \times 10^{-3}$	$4.3 \times 10^{-4} < \alpha_{GB} < 1.16 \times 10^{-2}$
$\sigma e^{-\kappa\phi}$	$N = 60$	$6.125 \times 10^{-4} \leq \alpha_{GB} \leq 9.141 \times 10^{-3}$	$8 \times 10^{-5} < \alpha_{GB} < 7.87 \times 10^{-3}$	$4.24 \times 10^{-4} < \alpha_{GB} < 1.3 \times 10^{-2}$

6 Conclusion

In this paper, we have considered a DBI model which is non-minimally coupled to a Gauss-Bonnet term. We have studied the cosmological dynamics of this model in the early times of the Universe history. We have calculated the inflationary parameters and the primordial density perturbations with details. If the DBI field is the only field in the inflation period as responsible for the inflation, the perturbations are adiabatic. But, in this paper since the DBI field interacts with the Gauss-Bonnet term, the isocurvature perturbations can be generated. Also, because of the non-minimal coupling between the DBI field and the Gauss-Bonnet term, the two metric perturbations are different. The non-Gaussianity of the primordial density perturbations in this model has been explored by studying the three point correlators. To this end, we have expanded the action up to the cubic order in the small fluctuations around the homogeneous background solution. Then, by using the interaction picture we have calculated the three point correlation functions. In the three point correlators, there are functions which depend on the momenta and are dubbed shape of non-Gaussianity. The momenta form a triangle and every shape has a pick in a configuration of triangle. In this work we have focused on the equilateral and orthogonal shapes which have a pick in $k_1 = k_2 = k_3$. We have expressed the leading-order bispectrum in terms of the equilateral basis S_*^{equil} and the orthogonal basis S_*^{ortho} and have found the amplitudes of the non-Gaussianity in the equilateral and orthogonal configurations. After obtaining the main equations, we have compared our setup with the recent observational data. We have taken the Gauss-Bonnet coupling as $\alpha(\phi) = \alpha_{GB} \mathcal{V}$ and have focused on the values of α_{GB} . We have considered two functions for $f(\phi)$ as $f = \beta\phi^{-4}$ and $f = \beta e^{\kappa\phi}$. For every f , we have adopted three potentials as $V(\phi) = \frac{\sigma}{2}\phi^2$, $\frac{\sigma}{4}\phi^4$ and $\sigma e^{-\kappa\phi}$ and for every potential we have considered three functions for \mathcal{V} as $\mathcal{V} \sim \phi^2$, ϕ^4 and $e^{\kappa\phi}$. By choosing these functions we have studied the evolution of the tensor to scalar ratio versus the scalar spectral index and the amplitude of the non-Gaussianity in the orthogonal configuration versus the equilateral configuration in the background of the joint Planck+WMAP9+BAO data. Also, we have obtained some constraints on the Gauss-Bonnet coupling term, α_{GB} that are summarized in tables. Our study shows that for $f = \beta\phi^{-4}$, the amplitude of the non-Gaussianity of the primordial perturbation in the model with a quadratic or exponential potentials and $\mathcal{V} \sim \phi^4$ lies outside the joint 95% CL of the Planck+WMAP9+BAO data. But, in some ranges of the Gauss-Bonnet coupling term, it is inside the joint 99% CL of the Planck+WMAP9+BAO data. Also, for $f = \beta e^{\kappa\phi}$ the amplitude of the non-Gaussianity of the model with a quadratic potential and $\mathcal{V} \sim \phi^4$ and with an exponential potential and $\mathcal{V} \sim e^{-\kappa\phi}$ is outside the joint 95% CL of the Planck+WMAP9+BAO data but inside the joint 99% CL of the Planck+WMAP9+BAO data in some ranges of α_{GB} . In other cases we have found the range of α_{GB} in which this setup is compatible with the observational data. Although our tables contain a variety of domains for α_{GB} , but inspection of these ranges show that the constraint $1.14 \times 10^{-5} \leq \alpha_{GB} < 4.5 \times 10^{-2}$ contains the most general domain for α_{GB} . In summary, in confrontation with recent data, the Gauss-Bonnet coupling α_{GB} is restricted to this domain.

Appendix A

$$S_3 = \int dt d^3x a^3 \left\{ \left[\frac{3H}{\kappa^2} + \frac{\dot{\phi}^2}{2\sqrt{1-f\dot{\phi}^2}} - \frac{f\dot{\phi}^4}{(1-f\dot{\phi}^2)^{\frac{3}{2}}} + \frac{f^2\dot{\phi}^6}{2(1-f\dot{\phi}^2)^{\frac{5}{2}}} - 80H^3\dot{\alpha} \right] \Phi^3 \right.$$

$$\begin{aligned}
& + \left[\left(144H^3\dot{\alpha} - \frac{9H^2}{\kappa^2} + \frac{3\dot{\phi}^2}{2\sqrt{1-f\dot{\phi}^2}} + \frac{3f\dot{\phi}^4}{2(1-f\dot{\phi}^2)^{\frac{3}{2}}} \right) \Psi - \left(\frac{6H}{\kappa^2} - 48H^2\dot{\alpha} \right) \dot{\Psi} - \frac{16H\dot{\alpha}}{a^2} \partial^2 \Psi \right. \\
& + \frac{2\kappa^{-2}H + 16H^2\dot{\alpha}}{a^2} \partial^2 B \left. \right] \Phi^2 + \left[\left(\frac{18H}{\kappa^2} + 216H^2\dot{\alpha} \right) \dot{\Psi} \Psi + \frac{16\dot{\alpha}}{a^2} \dot{\Psi} \partial^2 \Psi + \frac{\left(16H\dot{\alpha} - \frac{2}{\kappa^2} \right)}{a^2} \Psi \partial^2 \Psi \right. \\
& - \frac{2\kappa^{-2}H + 16H^2\dot{\alpha}}{a^2} \partial_i \Psi \partial_i B + \frac{\left(8H\dot{\alpha} - \kappa^{-1} \right)}{a^2} \left(\partial \Psi \right)^2 + \frac{12H\dot{\alpha} - \frac{1}{2\kappa^2}}{a^4} (\partial_i \partial_j B \partial_i \partial_j B - \partial^2 B \partial^2 B) \\
& + \frac{8\dot{\alpha}}{a^4} (\partial_i \partial_j B \partial_i \partial_j \Psi - \partial^2 B \partial^2 \Psi) - \frac{2\kappa^{-2}H + 24H^2\dot{\alpha}}{a^4} \Psi \partial^2 B + \frac{48H\dot{\alpha} - 2\kappa^{-2}}{a^2} \dot{\Psi} \partial^2 B \\
& + \left. \left(3\kappa^{-2} - 72H\dot{\alpha} \right) \dot{\Psi}^2 \right] \Phi + 8\dot{\alpha} \dot{\Psi}^3 + \frac{\kappa^{-2} - 8\ddot{\alpha}}{a^2} \Psi \left(\partial \Psi \right)^2 + \left(72H\dot{\alpha} - 9\kappa^{-2} \right) \dot{\Psi}^2 \Psi \\
& + \frac{2\kappa^{-2} - 16H\dot{\alpha}}{a^2} \dot{\Psi} \partial_i \Psi \partial_i B - \frac{8\dot{\alpha}}{a^2} \dot{\Psi}^2 \partial^2 B + \frac{2\kappa^{-2} - 16H\dot{\alpha}}{a^2} \dot{\Psi} \Psi \partial^2 B - \frac{2\kappa^{-2} - 16H\dot{\alpha}}{a^4} \partial_i \Psi \partial_i B \partial^2 B \\
& + \frac{\left(\frac{3}{2\kappa^2} - 12H\dot{\alpha} \right) \Psi - 4\dot{\alpha} \dot{\Psi}}{a^4} (\partial_i \partial_j B \partial_i \partial_j B - \partial^2 B \partial^2 B) \left. \right\}. \tag{106}
\end{aligned}$$

References

- [1] A. Guth, Phys. Rev. D, **23**, 347 (1981).
- [2] A. D. Linde, Phys. Lett. , **108 B**, 389 (1982)
- [3] A. Albrecht and P. Steinhard, Phys. Rev. D, **48**, 1220 (1982).
- [4] A. D. Linde, *Particle Physics and Inflationary Cosmology* (Harwood Academic Publishers, Chur, Switzerland, 1990). [arXiv:hep-th/0503203].
- [5] A. Liddle and D. Lyth, *Cosmological Inflation and Large-Scale Structure*, (Cambridge University Press, 2000).
- [6] J. E. Lidsey et al, Abney, Rev. Mod. Phys., **69**, 373, (1997).
- [7] A. Riotto, [arXiv:hep-ph/0210162].
- [8] D. H. Lyth and A. R. Liddle, *The Primordial Density Perturbation* (Cambridge University Press, 2009).
- [9] J. M. Maldacena, JHEP, **0305**, 013, (2003).
- [10] N. Bartolo, E. Komatsu, S. Matarrese and A. Riotto, Phys.Rept., **402**, 103, (2004).

- [11] X. Chen, Adv. Astron. **2010**, 638979, (2010).
- [12] A. De Felice and S. Tsujikawa, Phys. Rev. D, **84**, 083504, (2011).
- [13] A. De Felice and S. Tsujikawa, JCAP, **1104**, 029, (2011).
- [14] D. Babich, P. Creminelli and M. Zaldarriaga, JCAP, **0408**, 009, (2004).
- [15] C. Cheung, P. Creminelli, A. L. Fitzpatrick, J. Kaplan and L. Senatore, JHEP, **0803**, 014, (2008).
- [16] Y. Wang, [arXiv:1303.1523 [hep-th]].
- [17] D. Langlois, [arXiv:1102.5052 [astro-ph.CO]].
- [18] E. Komatsu, D. N. Spergel and B. D. Wandelt, Astrophys. J. **634**, 14, (2005).
- [19] P. Creminelli, A. Nicolis, L. Senatore, M. Tegmark and M. Zaldarriaga, JCAP, **0605**, 004, (2006).
- [20] M. Liguori, F. K. Hansen, E. Komatsu, S. Matarrese and A. Riotto, Phys. Rev. D, **73**, 043505, (2006).
- [21] A. P. S. Yadav, E. Komatsu and B. D. Wandelt, Astrophys. J., **664**, 680,(2007).
- [22] B. Zwiebach, Phys. Lett. B, **156**, 315, (1985).
- [23] D. G. Boulware and S. Deser, Phys. Rev. Lett., **55**, 2656, (1985).
- [24] S. Nojiri, S. D. Odintsov and M. Sasaki, Phys. Rev. D, **71**, 123509, (2005).
- [25] S. Nojiri, S. D. Odintsov and P. V. Tretyakov, Phys. Lett. B, **651**, 224, (2007).
- [26] Z. K. Guo and D. J. Schwarz, Phys. Rev. D, **80**, 063523, (2009).
- [27] Z. K. Guo and D. J. Schwarz, Phys. Rev. D, **81**, 123520, (2010).
- [28] R. A. Brown, *Brane world cosmology with Gauss-Bonnet and induced gravity terms*, (PhD Thesis, 2007), [arXiv:gr-qc/0701083].
- [29] K. Bamba, Z. K. Guo and N. Ohta, Prog. Theor. Phys., **118**, 879, (2007).
- [30] K. Andrew, B. Bolen and C. A. Middleton, Gen. Rel. Grav., **39**, 2061, (2007).
- [31] K. Nozari and B. Fazlpour, JCAP, **0806**, 032, (2008).
- [32] K. Nozari, and N. Rashidi, Int. J. Thoer. Phys., **48**, 2800, (2009).
- [33] K. Nozari, and N. Rashidi, JCAP, **0909**, 014, (2009).
- [34] K. Nozari, and N. Rashidi, Int. J. Mod. Phys. D, **19**, 219, (2009).
- [35] E. Silverstein and D. Tong, Phys. Rev. D, **70**, 103505, (2004).
- [36] M. Alishahiha, E. Silverstein, and D. Tong, Phys. Rev. D, **70**, 123505, (2004).

- [37] M. x. Huang and G. Shiu, Phys. Rev. D, **74**, 121301, (2006).
- [38] X. Chen, M. x. Huang, S. Kachru and G. Shiu, JCAP, **0701**, 002, (2007).
- [39] P. A. R. Ade et al., [arXiv:1303.5082].
- [40] P. A. R. Ade et al., [arXiv:1303.5084].
- [41] J. Bardeen, PRD, **22**, 1882, (1980).
- [42] V. F. Mukhanov, H. A. Feldman and R. H. Brandenberger, Phys. Rept., **215**, 203, (1992).
- [43] E. Bertschinger, [arXiv:astro-ph/9503125], (1995).
- [44] B. A. Bassett, F. Tamburini, D. I. Kaiser and R. Maartens, Nucl. Phys. **B**, **561**, 188, (1999).
- [45] C. Gordon, D. Wands, B. A. Basset and R. Maartens, PRD, **63**, 023506, (2001).
- [46] M. Bouhamdi-Lopez, R. Maartens and D. Wands, PRD, **70**, 123519, (2004).
- [47] N. Kaloper, PRD, **71**, 086003, (2005).
- [48] R. Maartens, D. Wands, B. A. Bassett and I. Heard, PRD, **62**, 041301, (2000).
- [49] D. Langlois, R. Maartens and D. Wands, Phys. Lett. **B**, **489**, 259, (2000).
- [50] D. Langlois and F. Vernizzi, JCAP, **02**, 017, (2007).
- [51] J. M. Bardeen, P. J. Steinhardt and M. S. Turner, PRD, **28**, 679, (1983).
- [52] D. Wands, K. A. Malik, D. H. Lyth and A. R. Liddle, PRD, **62**, 043527, (2000).
- [53] L. Amendola, C. Charmousis and S. C. Davis, JCAP **0612**, 020, (2006).
- [54] L. Amendola, C. Charmousis and S. C. Davis, JCAP **0710**, 004, (2007).
- [55] K. Nozari and N. Rashidi, Phys. Rev. D, **86**, 043505 (2012).
- [56] K. Nozari and N. Rashidi, Phys. Rev. D, **88**, 023519 (2013).
- [57] R. L. Arnowitt, S. Deser and C. W. Misner, Phys. Rev., **117**, 1595, (1960).
- [58] K. Koyama, Class. Quant. Grav., **27**, 124001 (2010).
- [59] D. Lyth and Y. Rodriguez, Phys.Rev. D, **71**, 123508, (2005).
- [60] D. Seery and J. E. Lidsey, JCAP, **0506**, 003, (2005).
- [61] X. Chen, M. x. Huang, S. Kachru and G. Shiu, JCAP, **0701**, 002, (2007).
- [62] A. Gangui, F. Lucchin, S. Matarrese and S. Mollerach, ApJ, **430**, 447,(1994).
- [63] L. Verde, L. Wang, A. F. Heavens and M. Kamionkowski, MNRAS, **313**, 141, (2000).
- [64] L. Wang and M. Kamionkowski, Phys. Rev. D, **61**, 063504, (2000).

- [65] E. Komatsu and D. N. Spergel, Phys. Rev. D, **63**, 063002, (2001).
- [66] D. Babich, P. Creminelli and M. Zaldarriaga, J. Cosmology Astropart. Phys., **8**, 9, (2004).
- [67] L. Senatore, K. M. Smith and M. Zaldarriaga, J. Cosmology Astropart. Phys., **1**, 28, (2010).
- [68] A. De Felice, S. Tsujikawa, JCAP, **03**, 030, (2013).
- [69] S. Tsujikawa, J. Ohashi, S. Kuroyanagi and A. De Felice, Phys.Rev.D, **88**, 023529, (2013).